Assessment of Roadway Surface Conditions Using Onboard Vehicle Sensors: Final Report

Phase I

www.its.dot.gov/index.htm

Final Report — March 2015
FHWA-JPO-16-359

U.S. Department of Transportation

Produced by Virginia Tech Transportation Institute (VTTI)

U.S. Department of Transportation

Office of the Assistant Secretary for Research and Technology

Notice

(Cover Photo: April Gray, Virginia Tech Transportation Institute)

Technical Report Documentation Page

1. Report No. FHWA -JPO-16-359	2. Government Accession No.	3. Recipient's Catalog No.
4. Title and Subtitle Assessment of Roadway Surface Conditions Using On-Board Vehicle Sensors: Final Report, Phase I		5. Report Date March 2015) 6. Performing Organization Code
7. Author(s) Cristian Druta, Ph.D. and Andrew S. Alden, P.E.		8. Performing Organization Report No.
9. Performing Organization Name And Address Virginia Tech Transportation Institute 3500 Transportation Research Plaza (0536) Blacksburg, VA 24061		10. Work Unit No. (TRAIS) 11. Contract or Grant No. DTFH61-13-P-00017
12. Sponsoring Agency Name and Address Federal Highway Administration Office of Joint Program 6300 Georgetown Pike McLean, VA 22101-2296		13. Type of Report and Period Covered Final Report, Dec 2012 - Aug 2014 14. Sponsoring Agency Code
15. Supplementary Notes Gabriel Guevara, COTR		

16. Abstract

Real-time assessment of road surface conditions can be used to provide valuable safety information to travelers when roads are slippery (e.g., contaminated roads, heavy rain, black ice, etc.). Identification of these hazardous surface conditions using onboard vehicle sensors will warn drivers to proceed with caution on compromised road sections, thus reducing the risks of crashes. This information may also be used to provide data on roadway deficiencies such as winter weather impacts and wear loss of surface friction to highway agencies resulting in more efficient and less costly maintenance operations.

The main objective of this study was to establish a real-time relationship between certain variables collected by vehicle onboard sensors and the roadway surface conditions. It is hypothesized that the relative difference in rotation between the driven and nondriven wheels may be used to assess pavement surface condition, and thus, traction.

Front- and rear-wheel drive vehicles were tested to determine the relative rotational displacements of driven and nondriven wheels under dry, wet, snowy/slushy, and icy road surface conditions. These variables, among others, were supplied by the factory-installed wheel-speed sensors utilized by the vehicle's Anti-lock Braking System (ABS). The rear-wheel drive vehicle was driven over two pavement sections of different grades and lengths to compare results. The front-wheel drive vehicle was driven on a single pavement section at the Virginia Tech Transportation Institute's Smart Road facility. Both vehicles were driven under controlled conditions of constant speed, minimal steering, no braking, and with monitoring of onboard safety systems (e.g., ABS, stability control) as potential confounds. Time and position data were collected from a Differential Global Positioning System (DGPS) installed in the vehicles. All these data were employed to calculate total distances traveled by the vehicles as well as ratios between distances traveled by driven and nondriven wheels in order to distinguish between different pavement surface conditions.

The results of experimentation with multiple test runs conducted on roads conditions ranging from dry to icy showed a small but statistically discernable difference in the relative rotational displacement of driven versus nondriven wheels. Changes in the observed rotation ratios were clearly associated with pavement conditions known to produce poor traction (e.g., icy, slightly wet and dirty). That is, tests performed on slippery roads resulted in an increased change in the driven versus nondriven wheel rotational rates. Of the surface condition scenarios tested, icy, and slightly wet and dirty, and certain snow-covered pavement provided the least traction while clean dry, moderately wet, and other snow-covered pavement conditions provided better traction.

17. Key Words Pavement friction, wheel sensor pulse, weather conditions, rotational displacement, traction, winter maintenance, Connected Vehicle	18. Distribution Statement No restrictions. This document is available through the National Technical Information Service; Springfield, VA 22161.		
19. Security Classif. (of this report) Unclassified	20. Security Classif. (of this page) Unclassified	21. No. of Pages 62	22. Price

Form DOT F 1700.7 (8-72) Reproduction of completed page authorized

U.S. Department of Transportation
Office of the Assistant Secretary for Research and Technology
Intelligent Transportation Systems Joint Program Office

Table of Contents

List of Tables

List of Figures

Chapter 1. Introduction

Background

Road friction develops at the contact patch between the tire and the pavement surface as the tire is driven or just freely rolls (Moore 1975) (Milliken 1995) (The Pneumatic Tire 2006) The force generated in the process, also known as skid resistance or skid friction, usually resists vehicle movement without the tire sliding. This force has an essential role in keeping vehicles safe on the road and is thus a vital component of traffic safety (Henry 2000) (Gillespie 1992) (Noyce 2007) (Pacejka 2012) (Rajamani 2012) . Over the years, it has been established that there is a correlation between highway crashes and pavement surface conditions, especially in slippery road conditions such as dirty roads or black ice (Hall 2009). In the United States, due to these slick surface conditions, it is expected that the number of crashes will remain at current levels or increase (Askelson 2008).

Recent data on traffic-related crashes in the United States have shown that the fatality rate is still high, with more than 100 fatalities occurring every day (Noyce 2007). It has been estimated that approximately 24 percent of all vehicle crashes have occurred in adverse weather conditions, resulting in about 7,400 deaths and 675,000 injuries on average per year (Murphy 2012) (Pisano 2011). A slick pavement surface is cited as a primary cause of 35 percent and a contributing cause of 63 percent of these adverse weather crashes, with nearly a quarter of these crashes occurring on roads covered by snow or ice (Knight 2008).The total economic costs of weather-related crashes exceeded $55 billion in the year 2000 and likely far exceeds that amount presently (IIHS Status Report 2010) (Blincoe 2002). At the same time, road maintenance agencies spend more than $2.3 billion annually on snow and ice control operations (Askelson 2008) (Rall 2012).

Under these compromised surface pavement circumstances, it is anticipated that the increased utilization of modern vehicle-based safety systems such as Anti-lock Braking Systems (ABS), Electronic Stability Control (ESC) systems, and Traction Control Systems (TCS) will mitigate the number and severity of crashes. However, many vehicles are still not equipped with these systems. Even when present, these systems are only able to assist to a degree because, ultimately, the steering or stopping ability of a vehicle is limited by the frictional force existing between tires and pavement.

Basics of Tire–Pavement Interaction

Prior anecdotal research conducted at the Virginia Tech Transportation Institute (VTTI) employing instrumented vehicles indicated that the rotational displacement in the driven wheels as related to the distance traveled by a vehicle may vary with respect to roadway conditions such as incline and tire grip. This could lead to a greater number of rotations of the driven wheels when compared to the free-rolling (or nondriven) wheels over the same travel distance. This phenomenon, known as “slip,” occurs because of the relative motion that develops between the tire and the road surface.

Typically, there are two types of slip that occur at the tire–pavement interface (i.e., contact patch): micro-slip and macro-slip. *Micro-slip*, or partial tire sliding, occurs when only a portion of the contact patch moves relative to the pavement and appears to increase when the coefficient of friction between tire and pavement decreases, as illustrated in **Error! Reference source not found.**. This means that the "static" and "sliding," or "dynamic" regions, will expand or contract depending on the degree of slipperiness of the road surface, vehicle speed, and level of braking. It is envisioned that this type of slip, which leads to diminished tire grip, could be quantified in real-time by the wheel-speed sensors prior to exceeding the macro-slip threshold that would activate the vehicle's onboard safety systems (e.g., ABS, ESC, etc.).

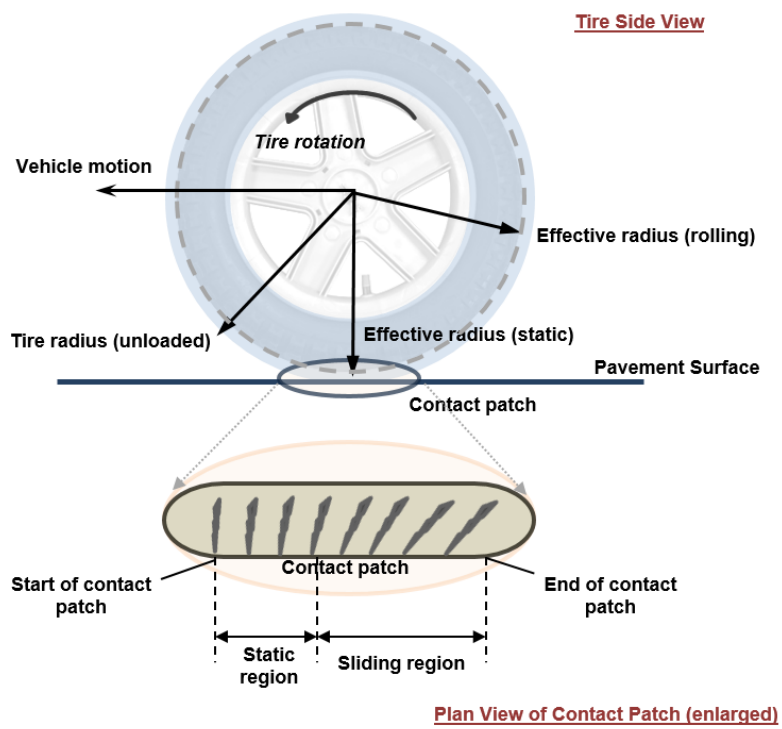

Source: VTTI

Figure 1. Example of micro-slip at the tire-pavement contact patch

The variables in Figure 1 are defined as follows:

Ground forces = Forces acting in opposition to tire rolling

V_x = Constant longitudinal velocity

r_{eff} = Wheel effective radius

r_s = Wheel static radius

r_f = Wheel undeformed radius

ω_w = Wheel rotational velocity

In the bottom portion of Figure 1, it can be observed how the tread elements are bending forward as they enter the contact patch in the case of the ***driven*** wheel (i.e., applied driving torque). For this case, the net velocity at the treads is given by the difference between the wheel rotational velocity ($r_{eff}\omega_w$) and its actual, constant longitudinal velocity (V_x). Figure 1 shows the relationship between these three parameters for the case of the driving wheel:

$$r_{eff}\omega_w > V_x$$

Figure 1. Equation. Tire longitudinal slip.

where, r_{eff} is the effective tire radius and ω_w is the rotational velocity of the wheel. The ($r_{eff}\omega_w$ - V_x) difference is also known as the tire *longitudinal slip* (Rajamani 2012) (Heising 2011).

Furthermore, the tip of the treads has zero speed in the static area of the contact patch as no sliding occurs in this region. In this case, as the rotational (or angular) velocity of the wheel increases, the contact patch tends to move forward with respect to the center of the wheel as a driving force is created in the process. Also, a circumferential compression occurs in the front of the tire when the tread enters the contact patch, which causes speed variations, and as a result of the speed variations, the distance that the tire travels may be less than the distance traveled by a free-rolling wheel. Early experimental work has shown that the effective rolling radius r_{eff} is usually smaller than the undeformed tire radius, r_f, but greater than the static vertical deflection of the tire, r_s such that $r_f > r_{eff} > r_s$ (Moore 1975) (Pacejka 2012). Similarly, there are longitudinal slip forces (i.e., ground forces or tire rolling resistance forces) at the front and rear tires acting in opposition to the longitudinal slip defined above. These are friction or reaction forces from the pavement acting on the tires to counterbalance the tire slip in the contact area. If the pavement surface cannot sustain the tire slip, then the wheel will slide instead of rotate.

As for the ***nondriven*** or ***free-rolling*** wheel, its longitudinal velocity is greater than the rotational velocity (i.e., $V_x > r_{eff}\omega_w$). It is worth pointing out that a longitudinal slip will always be present at the tire-pavement interface whether the vehicle is subject to driving, braking, or is in a cruising mode (Blundell 2004). As mentioned above, the tire radius decreases to an effective rolling radius (r_{eff}) due to the compression occurring as the tread approaches the beginning of the contact patch. As the tread enters the contact patch, its rearward tangential velocity (i.e., $r_f\omega_w$) relative to the center of the wheel is slightly greater than the vehicle's forward velocity, which causes an initial rearward slip in this region. Further into the patch, at the point where the undeformed radius (r_f) is reduced to its effective rolling value (r_{eff}), the forward vehicle velocity will equal the rearward tangential velocity. Hence, this point will be considered a zero-slip point as the longitudinal slips cancel each other (i.e., change direction) due to a shift in tire radii. As the tire radius further decreases to a static or "loaded" value $r_s < r_{eff}$, (at the center of the patch, Figure 1), the longitudinal slip is reversed to the vehicle's forward direction. In the last portion of the patch, the change in radius back to its undeformed state (r_f) when exiting the patch again causes a reverse in slip to a rearward direction. Consequently, the longitudinal slip changes direction several times during the course of this repetitive process as the tire moves through the contact patch, modifying it, and creating a so-called "squirm effect" along the way (Blundell 2004) (Wong 2001) (Savaresi 2010) (Gustaffson 1997) (Muller 2003) (Singh 2013).

Typically, the transition from the “static/sticking region” to the “slipping” or “sliding” region is regulated by the relative speed that develops at the tire–pavement interface (H. A.-Q. Wang 2010) (Clark 1971) (Wayson 1998).Moreover, the performance of a vehicle’s tires is strongly influenced by the local effects at the contact patch, such as tread deformations, as most of the transmitted forces depend on the frictional properties of both the tire and the pavement’s surface characteristics. These forces have to be transmitted reliably by the tire, not only on various pavement surfaces but also under different weather conditions and across a wide range of speeds (Henry 2000) (Heising 2011) (Smith 2008) In this respect, the force transfer between the tires and pavement is mainly achieved through two types of friction:

- Adhesive friction, which acts at the intermolecular level between the tire and pavement surface; and

- Hysteretic friction, which acts through interlocking forces between the tire and pavement surface.

Other types of friction, such as cohesive (tire wear) and viscous (over a thin water or oil film), do not have a significant impact on tire behavior. Adhesive friction requires a direct contact between the tire tread and the pavement surface and is the result of the small-scale bonding between the two. This component is predominant on dry surfaces (i.e., larger than hysteresis), as any contaminant present on the road, such as water or oil, will prevent direct contact with the pavement surface. The absence of these adhesive forces at the contact patch will practically eliminate this friction component by reducing the real contact area due to the fact that the loading is transmitted through the contaminant’s molecules. Other factors involved with this dry friction component are temperature, tire load and pressure, type of deformation, vehicle speed, and driving conditions (e.g., acceleration, braking, etc.) (Wong 2001) (Savaresi 2010) (H. A.-Q. Wang 2010).

Conversely, the hysteresis force in the tire induced by the carcass deflection while in contact with the road controls the tire’s rolling resistance. Hysteresis is a viscoelastic phenomenon that is related to the tire’s ability to recover after being elastically deformed, a process that continues until the tire returns to its original shape after the deformation force vanishes. Furthermore, hysteretic friction depends highly on the amount of contact between the tire tread and the roughness of the pavement surface. As an example, a tire made of a material with a large damping coefficient will also have a higher friction coefficient (i.e., better grip) due to an increased hysteresis. (See references (Moore 1975) (The Pneumatic Tire 2006) (Heising 2011) (Blundell 2004) (Wong 2001) (H. A.-Q. Wang 2010) (Clark 1971) (Smith 2008) (Blau 2009) (Gabriel 2010) (Bullas 2004) (Persson 1998) for more details on the two friction components and other related information.) Hence, adhesion may largely govern the friction of the dry, fine-textured surfaces as it depends on the micro-level roughness of the aggregate particles or fine materials contained in the surface. Hysteresis, however, is the prevailing component on wet and coarse or rough-textured pavement surfaces. Also, whereas the adhesion force is responsible for providing good traction at low speeds, the hysteresis component is more prevalent at high speeds where pavement macrotexture plays a critical role (Moore 1975) (Noyce 2007) (Hall 2009).

On the other hand, *macro-slip* takes place when the entire contact patch area “glides” or “skids” relative to the pavement’s surface (H. A.-Q. Wang 2010) (Wayson 1998). Generally, macro-slip occurrence may invoke a response from the vehicle’s safety systems (e.g., ABS, ESC, etc.) and could lead to potential loss of control or even crashes when the capabilities of these systems are exceeded. This phenomenon usually ensues under dynamic hydroplaning (no contact with riding surface due to

a thick water layer), viscous hydroplaning (over thin water films), aquaplaning (dirty roads), or on icy conditions (Moore 1975) (Pacejka 2012) (Blau 2009).(As an in-depth review of these phenomena is outside the scope of this research, additional information can be found in the literature (Blundell 2004) (Savaresi 2010) (H. A.-Q. Wang 2010).

From this standpoint, a comparison of the rotational displacement of the driven wheels to the distance traveled when using probe vehicles may provide an indication of the friction level of the pavement friction level and/or the road's slope. The slip due to road slope could be isolated to allow for calculation of pavement frictional characteristics (e.g., pavement surface slipperiness) if the incline and the distance traveled are known with sufficient accuracy. Measurement of either, to the degree of accuracy assumed required, is challenging at present and requires the use of additional technology such as a high-accuracy Global Positioning System (GPS; e.g., antenna dual-frequency, specific form factor, etc.). A description of a simpler, alternative method follows.

Chapter 2. Proposed Concept

A method for estimating road surface friction based on real-time tire micro-slip data using only the relative rotational displacement of driven and free-rolling wheels is proposed. As shown in Figure 2, the applied and reaction forces observed at the interface between the pavement's surface and the driven and free-rolling tires are opposed at constant road speeds.

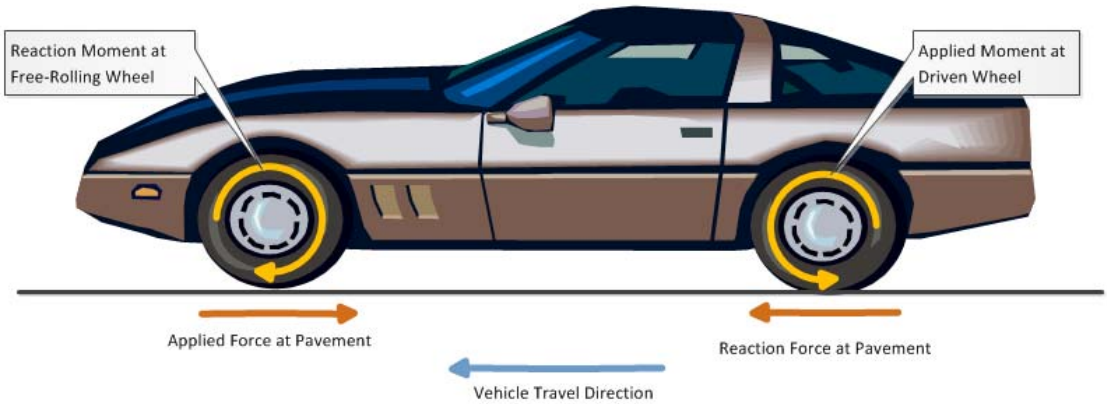

Source: VTTI

Figure 2. Diagram. Longitudinal forces occurring at wheels and pavement of a vehicle traveling at constant speed.

As a driven wheel rotates forward, it creates a reaction force at the pavement in the direction of travel. Conversely, the force applied to the free-rolling wheel by the pavement results in rotation of that wheel. The effect of slip that occurs at the driven and free-rolling wheels occurs in opposite directions such that a decrease in tire grip results in a greater differential in rotational displacement (i.e., the driven wheel turns more and the free-rolling wheel less). Therefore, the change in the relative rotational rates of driven versus free-rolling wheels should be predictive of changes in pavement friction.

Tire rotational rates may be affected by tire brand and construction, variations in size due to wear, loading, inflation pressure, brake and bearing drag, and other factors. However, because the proposed method uses only change in the relative rotation of driven versus free-rolling tires to predict relative changes in road friction, these factors do not adversely confound the method.

It should be noted that the effects of braking, acceleration, and road incline may introduce confounding factors that could challenge or invalidate this method. Acceleration, deceleration, and road slope change the normal forces between tire and pavement, resulting in altered frictional forces. The use of accelerometers to measure apparent linear acceleration due to road incline, braking, or

acceleration may be required in these circumstances. Apparent linear acceleration is typically measured by onboard accelerometers reporting to the vehicle Controller Area Network (CAN) bus.

Furthermore, the activation of all-wheel drive (AWD) or four-wheel drive (4WD) on vehicles equipped with these systems provides an obvious challenge to assessment using this method. If all four wheels are driven equally, the differential displacement between front and rear wheels will be minimized, effectively defeating the method. Therefore, this method would not work on vehicles equipped with full-time AWD. On those vehicles equipped with self-engaging AWD, the respective electronic control unit will enable the additional axle based on sensed wheel slip at the driven axle. Drivers of manually engaged 4WD vehicles will enable the additional drive axle based on their observations of road conditions. In either of these latter two scenarios, the method proposed herein would still be useful for predicting slip prior to the point at which either onboard controls (AWD) or the driver (4WD) have confirmed excessive (macro) tire slip.

Project Objective and Scope

VTTI proposed to use on-road vehicle testing in controlled conditions to validate whether the relative measured rotational rates of vehicle wheels can be used to assess road surface friction in real-time. These tests were performed on the Virginia Smart Road in Blacksburg, Virginia. The Smart Road is a closed test track facility built to interstate specifications with capabilities for creation of rain, mist, snow, and ice on a variety of full-width test pavement sections. The Smart Road has the added advantages of existing, extensive characterizations of the road friction on its pavement sections and precise positioning capabilities afforded by a permanent differential GPS base station. A fully functional connected vehicle (CV) network consisting of 10+ dedicated short range communications (DSRC)-based roadside equipment (RSE) units and an optical fiber-based Ethernet backhaul strand also allow real-time transmission and collection of relevant data from test vehicles. Proposed testing was conducted seasonally and under different artificially created weather conditions to maximize the range of available road friction values.

Road Condition Evaluation Using Vehicle Sensors

In recent years, mobile measurement devices that can be integrated into vehicles (e.g., optical friction meters, infrared sensors, positioning systems) or built-in sensors such as the accelerometers in smartphones, other mobile devices have been used more often to assess road surface conditions (Erdogan 2007) (Haavasoja 2010) (Malmivuo, Friction Meter Comparison Study 2011, n.d.). Also, due to their sensing capabilities and computerized dashboards, modern vehicles can be considered “storehouses” capable of collecting real-time information about road and traffic conditions (Dawkins 2011) (Andersson 2007). Attempts have been made to utilize the information (e.g., wheel rotation sensor, torque) supplied by the vehicle’s safety systems (ABS, ESC, or other systems) in order to estimate the surface friction of the pavement or detect freezing road conditions. Precise evaluation of these conditions is critical during winter maintenance as they are a useful basis for optimizing the application of deicing materials (Smithson 2012) (Erkkilä 2012) (Pilli-Sihvola 2014). (For additional information about the use of wheel sensors and other devices to assess and monitor road surface conditions, see references (Erdogan 2007) (Alimasi 2012) (Boon 2002) (IRIBA 2012) (Malmivuo, Comparison Study of Mobile Optical Friction and Temperature Meters 2013) (Pyykonen 2013).)

However, the models and algorithms based on the information collected from such systems are still under development as various aspects of the road-condition-estimation process are still not fully understood. Some approaches for estimating road surface friction, such those based on force and torque, need thorough calibration and tuning as many other variables (e.g., vehicle weight, tire size, etc.) come into play during data acquisition (Smithson 2012) (Erkkilä 2012). These steps are necessary to develop proper validation methods and procedures for an accurate estimation of the surface friction. Swedish researchers have categorized the methods of estimating tire–road friction into two groups: direct and indirect. From their standpoint, the direct methods would require excitation and accurate data on the dynamics of tire–roadway contact (e.g., wheel forces, speed), whereas indirect methods rely on algorithms derived from a priori road measurements (Pilli-Sihvola 2014). Nevertheless, both groups of methods present certain limitations that make them difficult to implement into mass-produced vehicles.

Several studies by Kumagai et al., Carlson et al., and Petersen have investigated the potential use of pulses or ticks from wheel sensors to evaluate the road conditions and subsequently to control rapid tire slip during braking (deceleration), acceleration, and turning maneuvers on wet and icy roads (Kumagai 2000) (Carlson 2003) (Petersen 2003). The method relies on counting the number of pulses generated per wheel rotation or distance traveled under varying driving conditions so that wheel slippage and direction are determined. Further information is available in Hay (Hay 2005). Although improvements to the method have been provided in recent years, only the augmented technique, which is coupled with GPS data, has proven to be an effective navigation assistance method to drivers in difficult environments (e.g., tunnels, tall buildings) rather than a road condition assessor. This drawback is mainly due to excessive signal noise due to ABS internal friction and other phenomena that are supplied by the wheel-speed sensors. To mitigate the noise problem, some researchers have used the Fast Fourier Transformation (FFT) processing method. The FFT method is applied to the wheel-speed signal to transform the signal into a frequency domain, which then transforms “filtered” waveforms into a real signal (L. M. Wang 2014). Other surface friction evaluation studies using a similar approach have been conducted in recent years on roads covered by snow and ice (Erkkilä 2012) (Petersen 2003) (Nakatsuji 2003). In these studies, slip ratios, defined as the relative speed difference between the vehicle and the front/rear wheels, were computed and analyzed to estimate the condition of the road surface for winter maintenance. Additionally, in order to determine the road conditions, researchers converted the wheel pulses into wheel speeds for various driving speeds (e.g., GPS speeds) using interpolation methods and conversion formulas. Major drawbacks in these studies were related to inaccuracies in data collection, especially for wheel pulses measurements, too long testing periods and road sections, poor correlation among measured variables, and the extensive calibration required for different sizes of probe vehicles.

Chapter 3. Methodology

Five tasks were to be completed in Phase I to provide the "proof of concept":

- Installation of vehicle instrumentation.
- Preliminary testing.
- Smart Road testing.
- Data analysis.
- Statistical analysis.

These five tasks are discussed in detail below.

Task 1: Installation of Vehicle Instrumentation

In this task, a 2008 Chevrolet Tahoe sport-utility vehicle (SUV) and a 2012 Chevrolet Impala sedan were used as the test vehicles. The SUV was rear-wheel drive (RWD) and equipped with a four-speed automatic overdrive transmission and a four-wheel ABS. The Chevrolet Impala was an automatic front-wheel-drive (FWD) vehicle with four-wheel ABS, an independent suspension, and traction and stability control. Both vehicles, pictured in Figure 3 and Figure 4, respectively, were equipped with the instrumentation necessary to acquire specific road test data.

Source: VTTI

Figure 3. Photo. RWD vehicle – Chevrolet Tahoe.

Source: VTTI

Figure 4. Photo. FWD vehicle – Chevrolet Impala. Testing kit installed in the back seat.

This instrumentation included the following components, which are interconnected within the vehicle.

- VTTI's NextGen data acquisition system (DAS).
- Vehicle CAN bus interface module (for communication inside the vehicle).
- A windshield-mounted head unit incorporating inertial measurement sensors for linear and angular acceleration.
- Standard GPS with real-time differential correction (DGPS).
- Laser system.
- A forward-looking camera to capture experimental procedures.

NextGen DAS

The NextGen DAS is a data acquisition system developed at VTTI that can be mounted on any commercial vehicle (e.g., car, truck, SUV, etc.) to capture a wide variety of performance measures (parameters) that can be used to evaluate its safety and operational performance. As pictured in Figure 5, this is a modular data collection system that can be configured for almost any research

application. The system includes a communications network and protocols, as well as data handling/storage capabilities such as a solid-state drive (SSD). A detailed list of the variables collected by the DAS is provided in the Data Acquisition section.

Source: VTTI

Figure 5. Photo. NextGen DAS showing SSD enclosure partially inserted at right side.

Moreover, the software applications include all of the necessary functions to support efficient transfer of collected data from vehicles to a data storage center (using the SSD) for accurate data analysis and access. Figure 6 and Figure 7 show an SSD and a drive reader used to download data collected through the DAS/Network box (shown below) onto a server, respectively. Both units were developed internally at VTTI by the data acquisition group. Software for use in the DAS units is being regulated by researchers' needs and complemented by supplying and integrating data triggers for use in data collection. This feature helps to ensure that the relevant vehicle parameters are extracted and communicated correctly, and the vehicles report valid values for these variables at the selected sampling rates.

Source: VTTI

Figure 6. Photo. DAS solid-state drive enclosure.

Source: VTTI

Figure 7. Photo. Solid-state drive reader.

In recent years, the system has been upgraded to provide increased data acquisition rates and throughput via updating the communication and processing hardware. The DAS now comprises several ports (e.g., USB, CAN, video, etc.), onboard wireless communication (e.g., cellular, Bluetooth), a 12-V DC power connection, and four video channels. The vehicle or CAN bus protocol allows various microcontrollers or devices to easily and efficiently communicate with each other inside a vehicle without being connected to a computer or network host.

Head Unit

The head unit, also developed at VTTI, is typically mounted on the windshield behind the rearview mirror and is set up to capture forward roadway, cabin, and face camera views (Figure 8). It comprises:

- 3-axis accelerometers.
- 3-axis gyroscopes.
- 3 cameras (e.g., forward, cabin, and rear).

Moreover, the unit can collect standard GPS data readings.

Source: VTTI

Figure 8. Photo. Head unit installed on windshield.

Differential Global Positioning System (DGPS)

The Differential Global Positioning System (DGPS) was a NovAtel system, FlexPak-G2 with OEMStar Global Navigation Satellite System (GNSS) receiver used to track the GPS L1, GLONASS L1, or combined GPS + GLONASS signals. Its customizable utility software supports automated receiver configuration and control, log decoding, specialized post-processing algorithms, and real-time data display. Communication was established through the OmniStar satellite service, which requires a dual-frequency receiver for improved accuracy. However, location accuracy depends on satellite geometry, local conditions, receiver capability, and other variables.

Source: VTTI

Figure 90. Photo. NovAtel DGPS receiver installed in experimental vehicle.

The system is also software upgradeable in the field, allowing for the custom performance required for on-demand applications. Figure 9 pictures the DGPS mounted in the rear of the SUV (behind the back seats) just above the DAS. The GPS antenna used with the system is shown in Figure 10. The OEMStar provides up to 14 channels of L1 GPS and GLONASS code and carrier phase tracking for better positioning and availability. Also, the receiver has a small form factor (the same as the OEMV-1 series), uses the OEMV-style command interface, and can be easily upgradable to the OEM615 GNSS receiver (a dual-frequency GNSS receiver). The Novatel GPS-702 GGL antenna that paired with the FlexPak-G2 system, provided single-frequency GNSS capabilities, permitting GPS and GLONASS signal reception.

Source: VTTI

Figure 10. Photo. GPS antenna installed on the top of experimental vehicle.

Network Box

The network box was a VTTI-developed, in-vehicle communication unit (Figure 11) designed to interface with a variety of vehicle network types, including the CAN bus and external sensors (e.g., laser, load detection, etc.) The box was located beneath the driver side dashboard and was communicating with the DAS and onboard computer. Standard variables collected with the network box included acceleration, braking, wheel rotation pulses, weather variables, and the status of onboard safety systems. During testing all collected data were stored on the DAS hard drive shown above.

Source: VTTI

Figure 11. Photo. VTTI DAS network interface box.

Laser Sensor

The Banner World-Beam QS30LPQ series photoelectric sensor was used to measure the exact distance traveled by the vehicle between two retroreflective markers installed on the pavement test section. The sensor, pictured in Figure 12, has far-limit cutoff (a type of background suppression) and fixed-field technology, allowing it to detect objects of low reflectivity placed directly in front of another surface (background). As the cutoff distance is fixed, the background or background objects beyond this distance are ignored. The laser sensor was installed at the left front of the experimental vehicle as shown in Figure 13.

Source: VTTI

Figure 12. Photo. Laser sensor used for delineation of test section.

Source: VTTI

Figure 13. Photo. Polarized laser sensor mounted on vehicle's front bumper.

A schematic layout of the data acquisition units being connected inside the vehicle is presented in Figure 14. It should be noted that other units (e.g., external sensors) can be connected to the DAS depending on the project requirements.

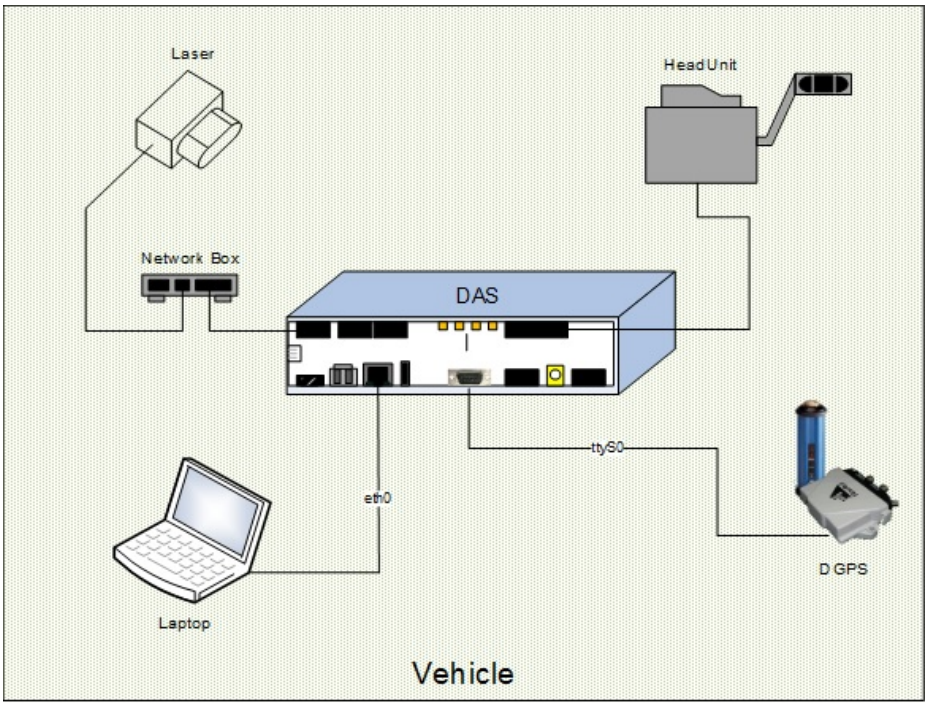

Source: VTTI

Figure 14. Diagram. DAS interconnection with in-vehicle sensors, DAS components, and laptop computer.

Weather Data Collection

Site weather data, such as pavement and air temperature, humidity, wind, etc., were collected using a **Kestrel 3000 pocket weather meter,** which is a handheld weather-monitoring device that provides a wide range of functions (Figure 15). This meter measures essential environmental parameters, such as temperature, wind speeds, and relative humidity, and features heat stress index and dew point. Additionally, an external temperature sensor and waterproof casing allow for gauging the temperature of air, water, and snow. The data could be used for comparison purposes when additional vehicles may be employed for similar testing.

Source: VTTI

Figure 15. Photo. Handheld weather meter.

Task 2: Preliminary Testing

This task was performed to validate test methods and data collection protocols before actual testing was conducted on the Smart Road under various weather and road conditions. This allowed "shakedown" testing of the instrumented vehicle without incurring the expenses and scheduling constraints associated with Smart Road utilization. The RWD vehicle instrumented in Task 1 was driven at different speeds to verify that the DAS was operational and data were recorded within required parameters. Data retrieval, upload to servers, and access were performed to validate test and data management methods. Differential corrections were reported by the GPS base station located at the Smart Road.

Distance Measurement Methodology

The aforementioned instrumented vehicle (i.e., the RWD Tahoe) with the laser sensor installed on the front bumper was evaluated to validate the sensing parameters. A short pavement segment of approximately 100 m, designated as the testing section, was delineated with two retroreflectors to determine if the vehicle traveled the correct distance. About 30 driving trips were executed from both directions to account for proper distance measurements while closely monitoring the acquisition statuses of other real-time parameters of interest such as the angular rotational displacement (i.e., wheel pulse count) and vehicle speed. This was necessary to ensure that all parameters' statuses would show correctly in the real-time Variable Inspection window and no communication losses that could lead to data corruption or invalidation would occur. Prior to collecting data, the laser sensor's sensing reliability had been verified for the best possible setup. For this purpose, several vehicle passes at constant speed were driven with the retroreflective elements positioned to maximize excess gain (in other words, the sensor-to-object distance should be such that sensing at higher excess gains makes maximum use of each sensor's available sensing power). Also, to avoid background light reflection back to the sensor, the two retroreflectors were angled horizontally as necessary.

During testing of traveled distance measurements, the vehicle's speed was maintained at a constant 35 mph throughout the entire section, including entering and exiting the delineated test section, while

steering input and brake application were kept at a minimum. All passes were driven at the designated vehicle speed with the driver attempting to retrace the same tire paths as in previous runs for consistency of the collected data. A schematic layout of the reflectors' positioning for the distance measurements is shown in Figure 16. The data acquisition process was triggered off when the vehicle passed in front of the reflector at the designated end of the segment. Collected DGPS, wheel speed and rotational displacements data were exported to a spreadsheet file for subsequent manipulation (e.g., data reduction, distance calculation, etc.).

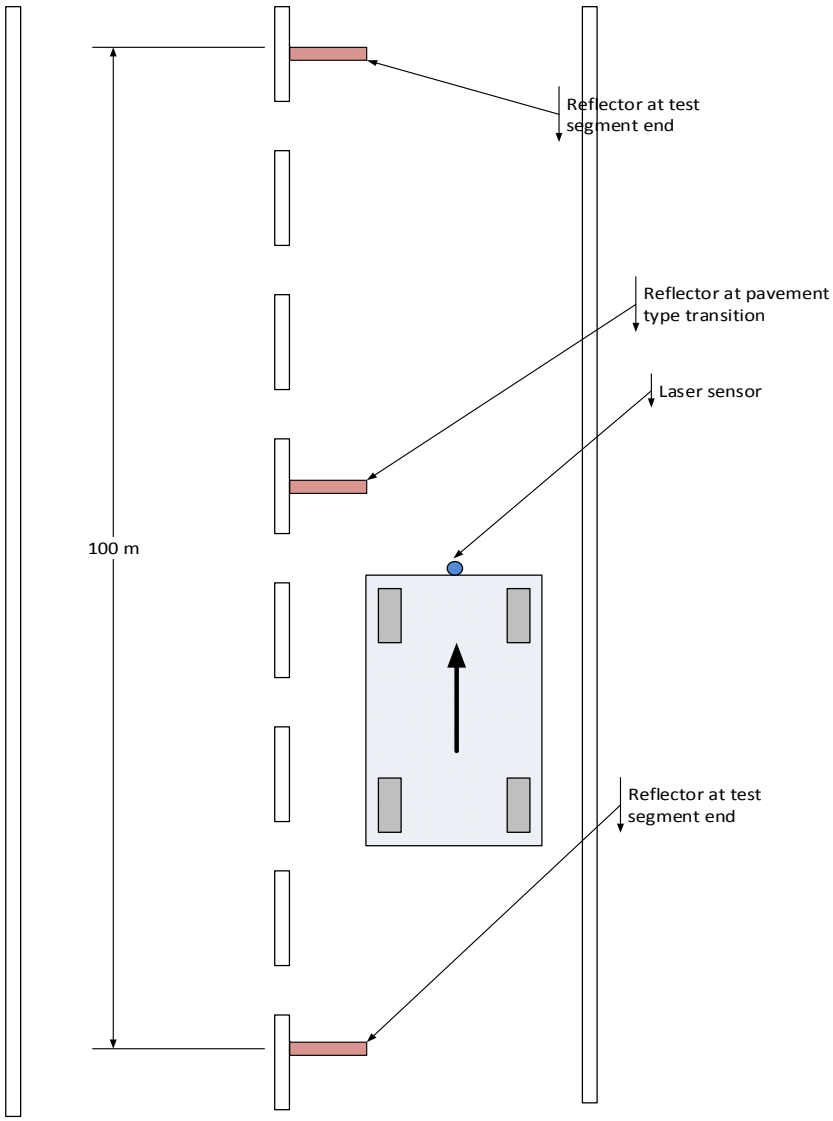

Source: VTTI

Figure 16. Diagram. Schematic showing distance-measurement procedure using laser sensor.

Experimental Data Acquisition

Recorded data included the following parameters that were retrieved from different data modules from the DAS:

- DGPS time and position – Real-time differential correction was used to provide sufficient accuracy for concept validation. Also, post-collection processing of raw GPS data was performed for additional positional accuracy/precision.
- Vehicle distance travel measured by the polarized retroreflective laser sensors (external sensor connected to DAS).
- Wheel rotation sensor pulse counts at all wheels (from the vehicle's CAN bus).
- Transmission output shaft sensor (vehicle speed; from the CAN bus).
- Status of ABS, ESC, and TSC. Activation of these systems during tests would likely affect the outcome and need to be recognized as a confounding influence (from the CAN bus).
- Brake activation and applied torque at all wheels (from the CAN bus).
- Throttle, both applied and actual. On "drive-by-wire" vehicles, input throttle and actual throttle may not be equivalent (from the CAN bus).
- Linear acceleration in the longitudinal and vertical axes for assessment of slope and/or vehicle acceleration. Preliminary tests should reveal whether additional gyroscopic data are required in the form of use of a full inertial measurement unit (IMU; from CAN bus).
- Variables indicative of atmospheric conditions such as temperature, wind speed, humidity, etc. (from portable weather device).

Relevant data of interest were transferred to a CV network located onsite from onboard equipment (OBE) operating in the test vehicle(s). The OBEs were provided by either VTTI and/or the Federal Highway Administration (FHWA). These data were collected at a time resolution dependent upon their availability from sensors, whether located on the CAN bus or installed by VTTI. Typical data rates ranged from 1 Hz to 1000 Hz.

All data modules were retrieved from the onboard DAS via solid-state storage and transferred to VTTI's data center for secure access and management. A proprietary VTTI-developed data viewer was used to extract and reduce relevant data for subsequent analysis from the data bases. This program tracks and opens up one data collection at a time that contains all the recorded data sets, then displays a list of certain variables and variable properties depending on the hard drive used for data collection (Figure 17). A "Search Variables" feature is available to allow the user to search for specific variables statuses.

Data Viewing – Real-time and Recorded

Figure 17 presents an example of real-time data collected and viewed using specialized software (the SOLEye program) developed at VTTI and installed on a laptop computer connected to the DAS. All these variables or modules are retrieved by the DAS from the vehicle's onboard computer. Moreover, the user has the option of browsing through the list of variables to select and check on the status and availability of relevant variables before the actual recording process commences. The Field Operation Test (FOT) Control variable enables the Start and Stop of the data acquisition routine during a driving trip. The Start-Record button was usually pressed once the optimal driving speed has been reached and all safety systems (e.g., ESC, TCS, etc.) turned off. This occurred at least 5 seconds before reaching the beginning of the road test section. Similarly, the Stop-Record button was pressed 5 seconds after exiting the test section. An ID number was assigned to each driving trip, in ascending order, and was keyed in to the SetDataRunNumber text box. A pre-driving session of 5 minutes was conducted each time before the actual data acquisition would commence, so that the tires would attain optimal temperature and pressure levels. These two parameters were continually monitored throughout the driving sessions to ensure consistent values for all trips.

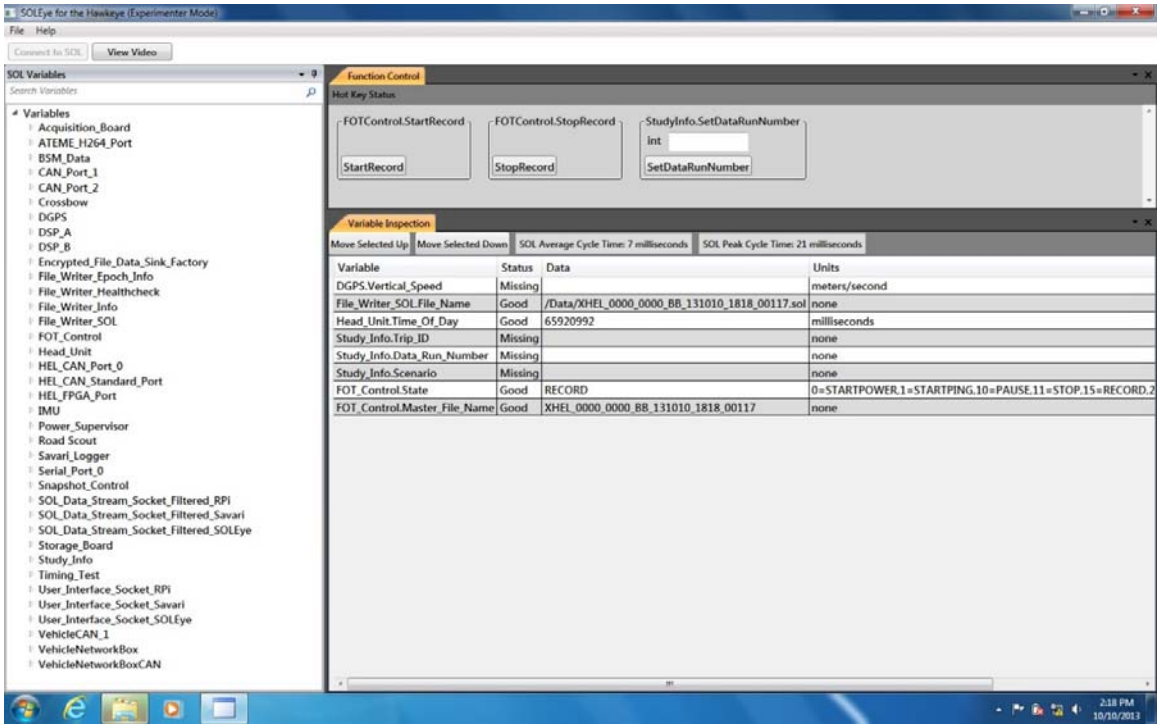

Source: VTTI

Figure 17. Screen capture. Real-time data collection and variable verification using SOLEye software.

Figure 18 shows a collection of variables such as DGPS_Measured_Distance, Left_Front_Tire_Distance, etc., selected from a recorded module (e.g., CVR_Control, DGPS, etc.) as displayed using the Hawkeye data viewer program, a VTTI proprietary software application. Highlighted cells indicate a Start Record data set (as shown in Figure 18) when the laser sensor was triggered at the beginning of each test segment. A time stamp, typically in milliseconds (ms), is recorded for each variable value under all the OBD modules. Other sampling rates may be available depending on the variable module.

Additional information, including videos, is available in Hawkeye regarding acquired data files such as vehicle and participant identification, collected date and time, file ID and length, and location code. Other data collection fields are available upon selection by the user from the database menu. Data pertaining to each variable can be viewed two ways: as a continuous data graph, where data are presented in a chart, or as a raw data graph, where data are presented in a tabulated form (as illustrated in Figure 18). Tabulated data can be copied and pasted into a spreadsheet file for further manipulation.

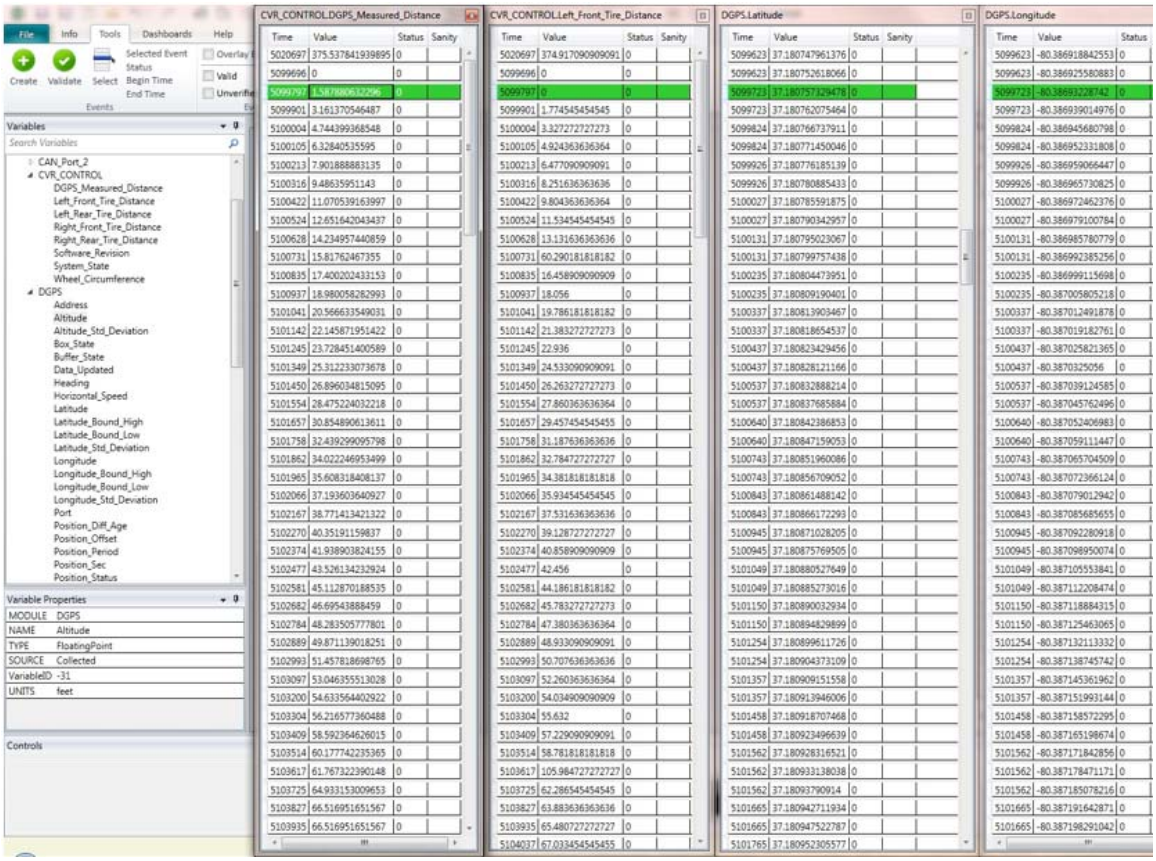

Source: VTTI

Figure 18. Screen capture. Variables recorded under various DAS modules and viewed using VTTI proprietary software (i.e., Hawkeye data viewer).

Task 3: Smart Road Testing and Data Collection

Once the instrumented vehicles equipped in Task 1 had been successfully tested in Task 2, it was decided to implement the same testing methodology on the Smart Road. For this purpose, an inclined and relatively straight portion of the road, about 300-m long, was selected for conducting the proposed measurements. The selected road segment is paved with hot-mix asphalt concrete and lies within the precipitation-making area. All initial measurements were conducted on dry pavement and in the uphill direction to maximize the micro-slip effect. About 30 passes were driven by the same driver under

similar conditions as the preliminary testing (i.e., same speed, minimal steering, and no braking) using the RWD vehicle. The deployment of the retroreflective markers for the laser sensor used to measure the distance traveled by the vehicle is shown in Figure 19 and Figure 20.

Source: VTTI

Figure 19. Photo. Retroreflectors installed at the beginning and end of test section.

Source: VTTI

Figure 20. Photo. Retroreflective markers installed on centerline of Smart Road.

Prior to starting the data collection, tire-related parameters such as temperature, pressure, and circumference were recorded. These parameters were also monitored throughout the entire testing session. Values for these parameters are presented in Error! Reference source not found.. Tire pressure was checked and adjusted every five trips, while onboard safety systems were monitored to ensure they were not activated during tests. The pressure was kept constant throughout the entire testing period. Additional information on tires, pavement, and weather conditions is provided in Appendices A and B.

Table 0-1. Tire-related parameters recorded during testing (Fall 2013).

Wheel	Tire pressure (psi)	Tire temperature (°C) Tread	Tire temperature (°C) Sidewall	Circumference (cm)
Left Front	37	23	24	249.7
Right Front	37	23	24	249.8
Left Rear	37	23	24	249.8
Right Rear	37	23	24	249.9

Source: VTTI

Data Collection

Specific primary collected variables, along with a description of their source and use, are listed in Table 0-2. Several of these variables were used to derive road slippage in the preliminary analysis of the acquired data. As a note, wheel pulses per revolution were available for front and rear axles for the RWD vehicle.

Table 0-2. Primary variables collected during testing.

Variable	Type	Module/Sensor	Notes
Time (ms)	Control	Across modules (CVR, DGPS, VehicleCAN_1)	Timestamp for every data set recorded
Vehicle Speed (m/s)	Control	DGPS, VehicleCAN_1	Constant during test
Tire Traveled Distance (m) (LeftFrontTire, RighFrontTire, etc.)	Control	DGPS, CVR_Control, Laser sensor	Laser sensor triggers data collection

Variable	Type	Module/Sensor	Notes
Vehicle Position (deg, m) (Latitude, Longitude, and Altitude)	Control	DGPS	Used for DGPS measured distance under CVR_Control
Wheel Distance Pulse Counter (counts) (LeftDriven, RightDriven, etc.)	Dependent	VehicleCAN_1 (ABS)	For the RWD vehicle only: Front: 55 counts/rev Rear: 32 counts/rev
Vehicle Safety Systems	Independent	Status from vehicle network	Monitored/Recorded to prevent activation
Brake System	Semi-control	Vehicle network box Brake light switch	Brakes should not be applied/Monitored to prevent activation
Site Weather	Independent	Handheld meter/ Onboard sensors	Monitored/Recorded (air temp., wind speed, dew point)

Source: VTTI

Preliminary Data Analysis

An example of the methodology used to calculate variables needed for preliminary analysis of the data is presented in Figure 22. In this example, the data have been collected from 30 uphill vehicle trips (only 7 shown) across three modules—CVR_Control, DGPS, and Vehicle CAN_1–on a dry pavement surface. Initial data analysis indicated, though, that several distance measurements were not accurate as the laser erroneously triggered the data collection process (i.e., either before or after passing by the retroreflector). Additional findings from the testing sessions are summarized in the lessons learned section. All calculations and statistical analyses were performed using the Microsoft Excel 2013 software.

PARAMETER / TRIP	2292_Up	2298_Up	2302_Up	2306_Up	2314_Up	2317_Up	2321_Up
DGPS CalcDistance (m)	302.5146815355	302.6507733672	302.3870267929	302.4256904860	302.3543120786	302.4684261211	302.4176396781
CalcDistance using Altitude	302.5511240147	302.6855033861	302.4255557804	302.4624343938	302.3915434452	302.5049269022	302.4549639973
PulseCount LFND - Start	983	174	44	982	435	681	709
Total # of 10-bit Counts LFND (1024)	6144	5120	5120	6144	6144	6144	6144
PulseCount LFND - End	653	859	744	641	118	338	367
Total # of Pulses - LFND	6838	6829	6844	6827	6851	6825	6826
PulseCount RFND - Start	107	386	430	787	356	350	798
Total # of 10-bit Counts RFND (1024)	5120	6144	6144	6144	6144	6144	6144
PulseCount RFND - End	794	39	98	439	32	0	449
Total # of Pulses - RFND	6831	6821	6836	6820	6844	6818	6819
PulseCount LRD - Start	706	894	12	790	737	873	997
Total # of 10-bit Counts LRD (1024)	3072	3072	2048	3072	3072	3072	3072
PulseCount LRD - End	597	779	930	676	637	756	880
Total # of Pulses - LRD	3987	3981	3990	3982	3996	3979	3979
PulseCount RRD - Start	897	72	253	921	886	266	622
Total # of 10-bit Counts RRD (1024)	3072	2048	3072	3072	3072	3072	3072
PulseCount RRD - End	785	977	143	803	782	145	502
Total # of Pulses - RRD	3984	3977	3986	3978	3992	3975	3976
Dist Calc from Pulses - LFND (m)	303.1098909091	302.7109454545	303.3758545455	302.6222909091	303.6861454545	302.5336363636	302.5779636364
Dist Calc from Pulses - RFND (m)	302.7996000000	302.3563272727	303.0212363636	302.3120000000	303.3758545455	302.2233454545	302.2676727273
Dist Calc from Pulses - Avg Front (m)	302.9547454545	302.5336363636	303.1985454545	302.4671454545	303.5310000000	302.3784909091	302.4228181818
Dist Calc from Pulses - LRD (m)	303.8841562500	303.4268437500	304.1128125000	303.5030625000	304.5701250000	303.2744062500	303.2744062500
Dist Calc from Pulses - RRD (m)	303.6555000000	303.1219687500	303.8079375000	303.1981875000	304.2652500000	302.9695312500	303.0457500000
Dist Calc from Pulses - Avg Rear (m)	303.7698281250	303.2744062500	303.9603750000	303.3506250000	304.4176875000	303.1219687500	303.1600781250
Absolute Slippage (AvgDistD - AvgDistND)	0.8150826705	0.7407698864	0.7618295455	0.8834795455	0.8866875000	0.7434778409	0.7372599432
Undriven/Driven Ratio	0.9973167754	0.9975574270	0.9974936551	0.9970875961	0.9970872668	0.9975472651	0.9975680837
DGPS CalcDistance/Dist Calc Pulses - Rear	0.9959880673	0.9980581848	0.9949505944	0.9970720660	0.9933441973	0.9979643777	0.9976741195
DGPS CalcDistance/Dist Calc Pulses - Front	0.9986677171	1.0005019839	0.9974505495	0.9999844246	0.9962459961	1.0004181382	1.0001062943
TotalPulsesUnDriven/TotalPulsesDriven	1.7148412997	1.7152550892	1.7151454363	1.7144472362	1.7144466700	1.7152376163	1.7152734129
TotalPulsesDriven/TotalPulsesUndriven	0.5831443412	0.5830036630	0.5830409357	0.5832783762	0.5832785688	0.5830096020	0.5829974350
RotSpeedDriven							
RotSpeedNonDriven							

Source: VTTI

Figure 21. Screen capture. Relative rotational displacement (slippage) calculated from DGPS measured distance and wheel pulses.

Because of the numerous unsuccessful attempts to remedy this unforeseen circumstance, it was decided to use the DGPS location variables (i.e., latitude, longitude, and altitude) instead to more accurately compute the traveled distance in the next testing stages. Additional calculated variable values for three different road surface conditions (e.g., light wet, very wet, etc.) are presented in the next section.

Relative Driven Displacement (RDD) and Relative Nondriven Displacement (RND) represent ratios of the DGPS-measured vehicle distance to average driven and nondriven wheel distances calculated using the total wheel number of pulses per total traveled distance, as shown in the equations in Figure 22 and Figure 23. As can be noted from Table 3, the calculations for RDD and RND, along with those for Relative Rotational Displacement (RRD), yielded values less than 1. These results indicate that, in actuality, the driven wheels generally travel further (i.e., rotate more, thus RDD < RND) over the same distance when going in an uphill direction, showing that the concept of micro-slippage holds under the proposed controlled testing conditions.

$$RDD = D_M / WTD_D$$

Figure 22. Equation. Relative driven wheel displacement.

where:

- D_M is the DGPS-measured distance (specified by the CVR module).

- WTD_D is the calculated average driven total wheel-traveled distance using the total number of pulses per wheel (N_p).

$$RND = D_M / WTD_N$$

Figure 23. Equation. Relative nondriven wheel displacement.

where: RRD = RDD/RND = WTD_N / WTD_D

- D_M is the DGPS-measured distance (specified by the CVR module).

- WTD_N is the calculated average nondriven total wheel-traveled distance using the total number of pulses per wheel (N_P).

RRD is the ratio of the averaged driven to averaged nondriven wheel distances calculated using the total wheel number of pulses per total traveled distance (Figure 24).

$$RRD = RDD/RND = WTD_N / WTD_D$$

Figure 24. Equation. Ratio of driven-to-nondriven wheel displacement.

RDD and RND are given by the equations shown in Figure 22 and Figure 23.

The average driven and nondriven total wheel-traveled distances (WTD_{WP}) are calculated from wheel pulses (WP) using the equation in Figure 25.

$$WTD_{WP} = N \times C$$

Figure 25. Equation. Wheel travel distance.

where:

- N is the total number of pulses per wheel traveled distance.

- C is the wheel circumference (measured per wheel before each testing session) in meters.

The total (cumulative) number of pulses (i.e., VehicleCAN_1 variables) per wheel traveled distance (N_p) can be calculated using the following equation (Figure 26):

$$N_P = (1024 - A) + (1024 * n) + B$$

Figure 26. Equation. Total wheel sensor pulses.

where:

- A is the number of wheel pulses corresponding to pavement section StartPoint (from VehicleCAN_1 module).

- 1024 is the maximum value of the 10-bit pulse counter supplied by the wheel rotation sensor. This number is between 0 and 1024.

- n is the number of complete 10-bit pulse counts per wheel for the traveled distance.

- B is the number of pulses corresponding to pavement section EndPoint (from VehicleCAN_1 module).

Task 4: Data Analysis and Discussion

Calculated Variables for the RWD Vehicle

Graphs of calculated average RRD values for all of the road surface conditions tested are presented in Figure 27 and Figure 28. All of the data were collected at a constant speed of 35 mph and in an uphill direction while driving on the Smart Road. Additional data collected on a primary road (U.S. 460-E) are presented in Figure 29 and Figure 30. Vehicle speed on US-460 highway was kept constant at 60 mph. The results are grouped by both ratios and surface conditions for 30 vehicle trips. The red line acts as a delineator indicating which ratios are larger than 1.

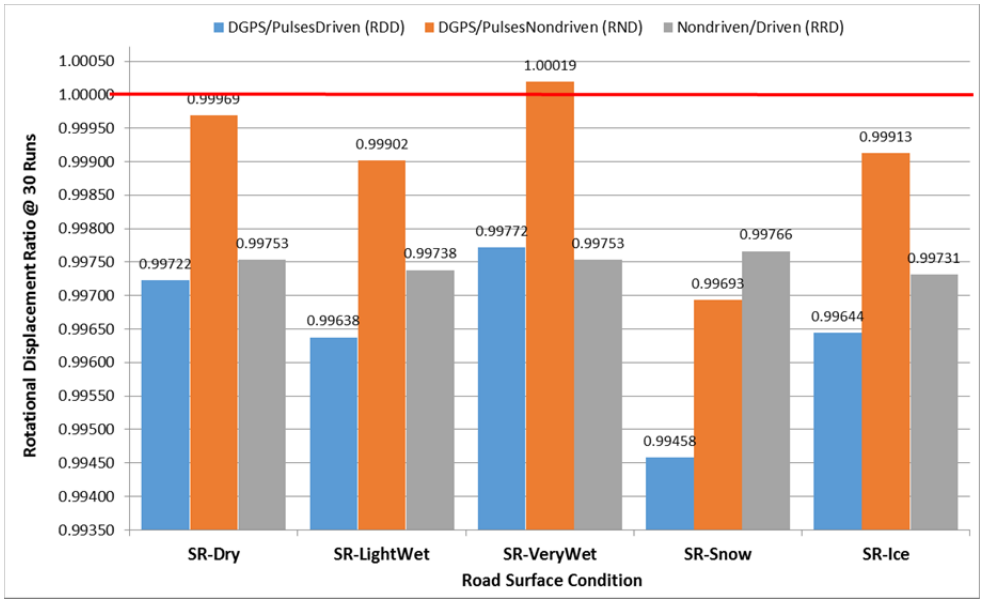

Source: VTTI

Figure 27. Chart. Calculated RRDs from wheel pulses (grouped by surface condition) using Smart Road data.

Ratios larger than 1 denote that more rotation occurred at the nondriven wheels compared to the driven wheels, showing that tire–pavement slip acts differently at each axle depending on the surface condition. Fresh snow depth was in the range of 2-4 inches and decreased to about 1 inch after 10 passes, while the ice layer was about 1/6 of an inch (i.e., 4-5 mm) thick.

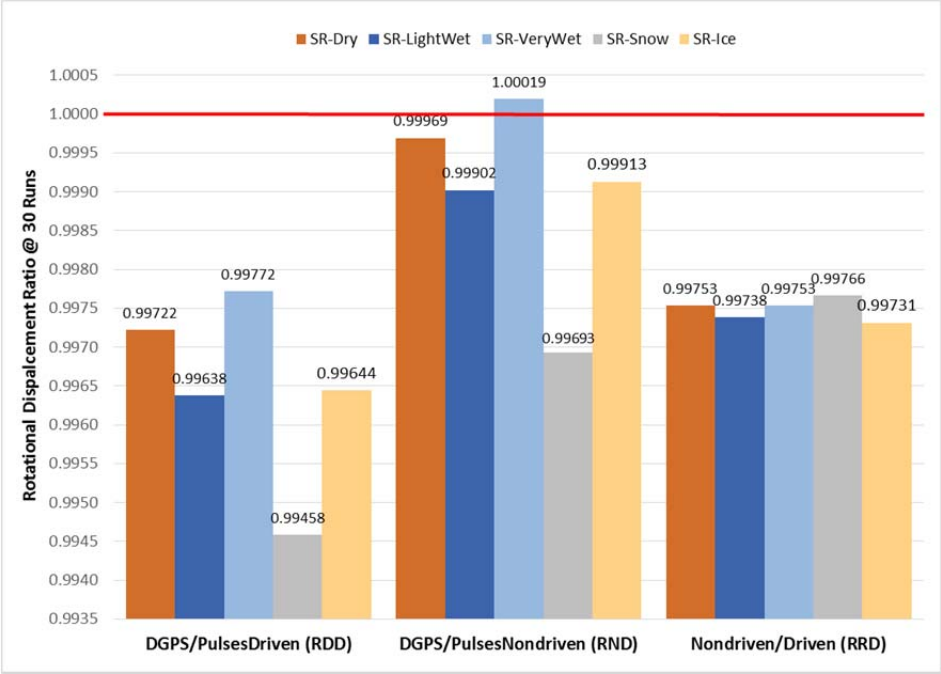

Source: VTTI

Figure 28. Chart. Calculated RRDs from wheel pulses (grouped by ratio) using Smart Road data.

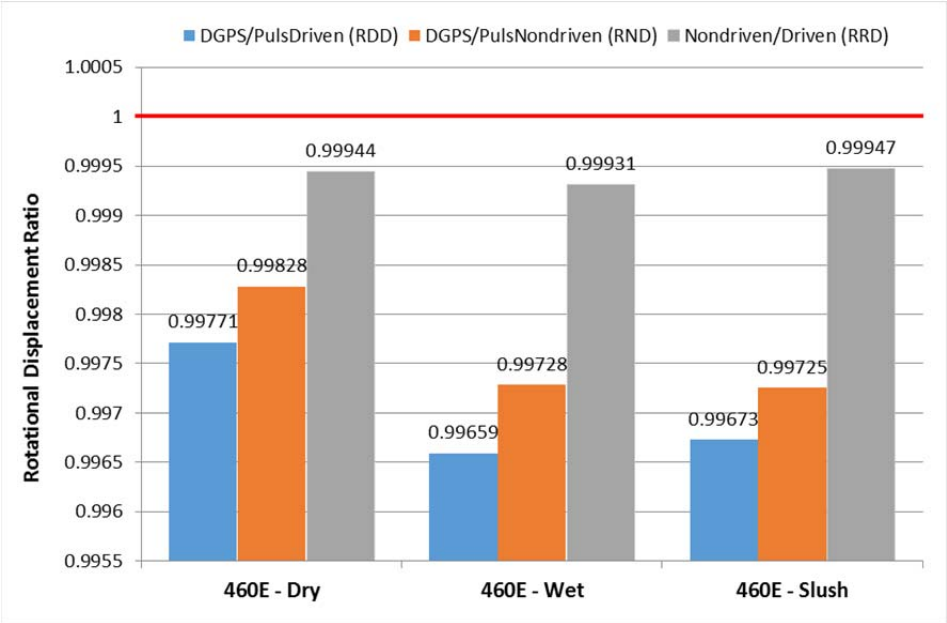

Source: VTTI

Figure 29. Chart. Average RRDs calculated from wheel pulses (460-E data grouped by surface condition).

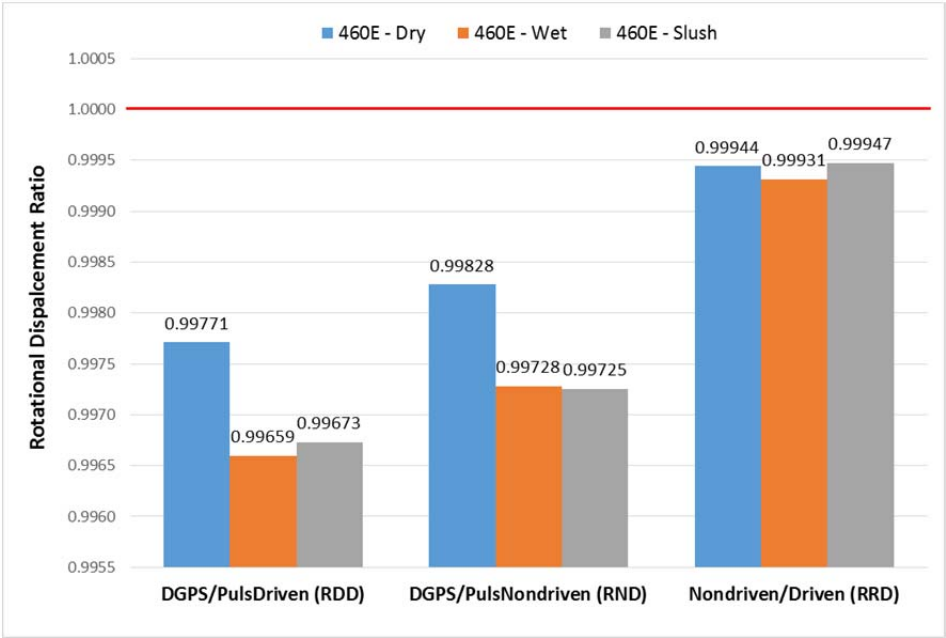

Source: VTTI

Figure 30. Chart. Average RRDs calculated from wheel pulses (460-E data grouped by ratio).

Figure 31 and Figure 32 show ratios of average values corresponding to the total number of pulses of the front (nondriven) and rear (driven) wheels while driving on the Smart Road and U.S. 460

eastbound, respectively. As most of today's vehicles are not currently equipped with a GPS, let alone a differential GPS, acquiring just the number of wheel pulses from various types of vehicles will provide more manageable data with respect to an accurate evaluation of the road condition. The SUV was driven on U.S. 460 over a distance of 1.5 miles. This road section was less inclined compared to the Smart Road section (i.e., it has around 2% slope).

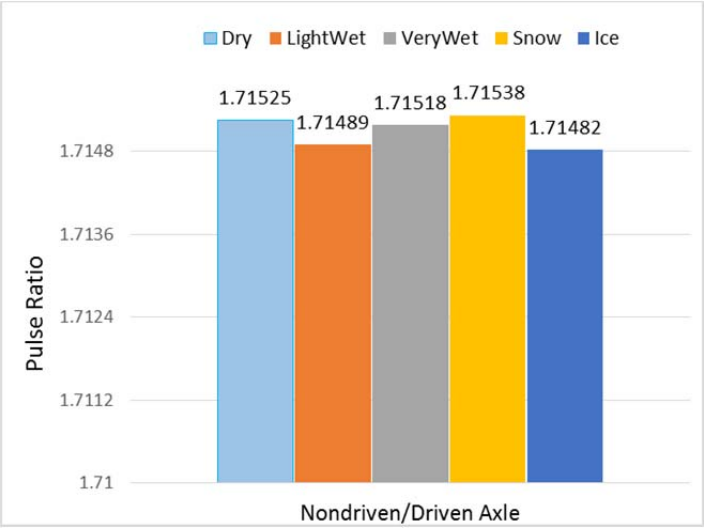

Source: VTTI

Figure 31. Chart. Ratios of total pulses of driven and nondriven wheels from data collected on Smart Road.

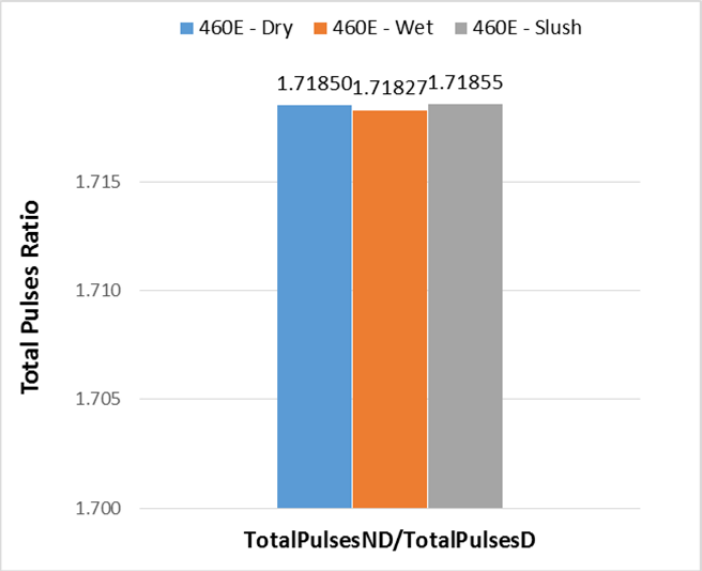

Source: VTTI

Figure 32. Chart. Ratios of total pulses of driven (D) and nondriven (ND) wheels from data collected on US 460E.

As anticipated, similar or slightly lower relative displacement values to those previously defined were obtained for tests conducted in the uphill direction on the selected pavement section in different surface conditions (e.g., dry, wet, snow, etc.) However, as most of the calculated parameters' values were less than 1, it can be inferred that under the different road-testing conditions that the vehicle's driven wheels would always travel further (e.g., rotate more) than the nondriven wheels (i.e., free rolling). From this standpoint, a rotational differential of the wheels can be provided over a short period of time, thus offering valuable information about the immediate road conditions in real-time. Data presented in the above graphs clearly indicate these trends in the variables. It should also be noted that as a vehicle moves along a roadway, front and rear wheels are spinning equally at constant linear speed (Gillespie 1992) (Noyce 2007). One factor that may have contributed to the distance ratios being so similar could have been the DGPS accuracy. It is believed that although the GPS data were collected at 20 Hz rate, a ± 2-3 inch difference might have existed among computed distances over the entire length of the tested section. These differences translated into small "bouncing" values obtained for the calculated distances across multiple trips conducted for a certain surface condition which were subsequently averaged.

As illustrated by the graphs, the most slippery road conditions were, as expected, the lightly wet and icy surfaces. This is in accordance with well-known observations from the literature that road surfaces tend to be more slippery after a light rain or shortly after it starts raining than after a heavy downpour. The explanation resides in the fact that a thin layer of dirt/mud forms on the surface of a dirty road after a light rain, whereas all the impurities and depositions are washed away during a downpour. At the same time, a slightly wet road surface exhibits lower frictional coefficients than a flooded pavement, especially at lower speeds (Henry 2000) (Pacejka 2012).

Similarly, the ice layer formed on the road surface exhibits air voids, cavities, impurities or contaminants, and undulations, thus providing an uneven riding surface with a variable density. Concurrently, the interlocking crystals in the ice structure are coated with a thin film of water at temperatures even below their melting point (Giessler 2010). This layer typically ensures transition from the rigid structure of the ice crystal arrangement to that of water. It also allows the refreezing of the water film formed on the surface of the ice through a process known as *regelation,* during driving. In this process, melting occurs at the ice–tire interface as the tire continually applies a certain amount of pressure to the ice sheet. Thus, load is transmitted through a thin water film similar to the lightly wet pavement condition when the coefficient of friction is very low. As the tire exits the contact patch, it allows the film to refreeze due to the sudden release of pressure. For situations when there is a drop in temperature, experimental work has shown that the friction increases as the melting of the water film becomes more difficult. At high speeds (e.g., over 40 mph), however, the frictional melting complements the pressure-melting process to generate the water layer.

On the other hand, a "cleaning effect" takes place while driving in rainy or slushy conditions as the front wheels clear the path thus, diminishing the water film in front of the rear wheels which leads to an increased traction. Similarly, improved traction may occur while driving in freshly snow-covered pavement for driven wheels as the front wheels compact the snow to create additional adhesive friction (less slip compared to icy conditions). This, in turn, may at times lead to more spinning of the front wheels (Rall 2012) (Heising 2011).

Calculated Variables for the FWD Vehicle

Similar graphical data collected with the FWD vehicle (i.e., Chevy Impala) are presented in Figure 33 and Figure 34. The data were collected following the same procedure as for the RWD vehicle (i.e.,

constant speed, minimal steering, and no braking). Also, the ESC and TCS were turned off throughout the driving sessions.

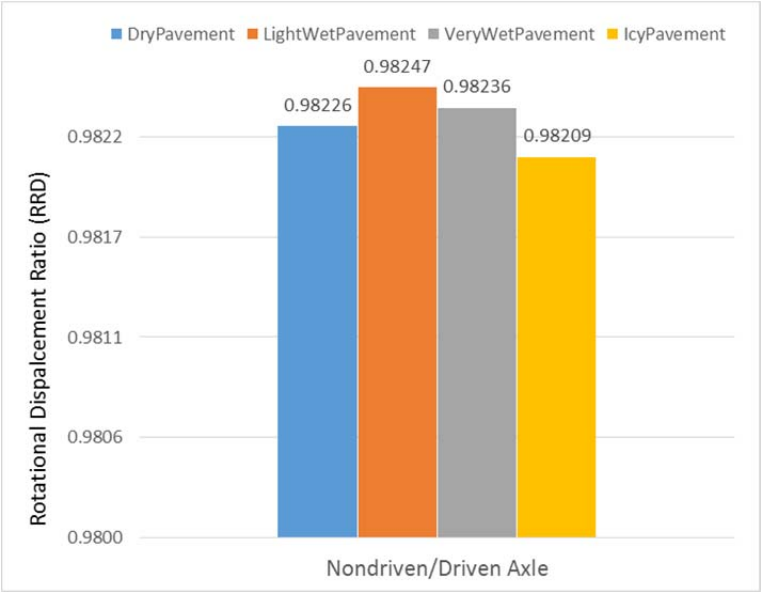

Source: VTTI

Figure 33. Chart. Calculated RRD for FWD vehicle.

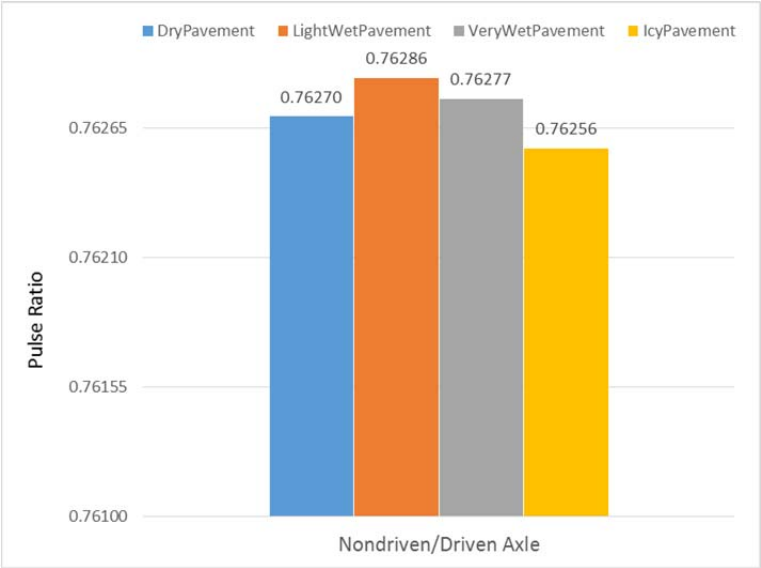

Source: VTTI

Figure 34. Chart. Pulse ratios of driven and nondriven wheels for FWD vehicle.

In this case, it appears that more spinning (slip) occurred at the rear wheels than at the front wheels (driven wheels) on the very wet surfaces compared to the RWD vehicle. As mentioned in the introduction, the performance of tires on wet surfaces depends on many parameters, both road

related as well as tire related, such as pavement surface texture, tread material, depth and pattern, water/snow layer thickness, and vehicle operating mode. For the FWD vehicle, traction is provided by the front axle (meaning more spinning) compared to the free-rolling rear axle as the tractive effort of the vehicle is controlled by tire–road adhesion, which is affected by the axle weight. A similar phenomenon occurs in the RWD vehicle when driving on ice; the driving axle spins more, indicating lower traction, which corresponds to a lower coefficient of friction. Furthermore, there exist fluctuations in the wheel rotation and speed signals (e.g., ABS signal) due to vibrations in the chassis as the wheel-base changes during travel, thus affecting the nondriven/driving ratios for different road conditions (Heising 2011) (Blundell 2004).

Task 5: Statistical Analysis

Sample Size Comparisons

A statistical power analysis was conducted to determine the sample size (i.e., the number of trips or passes) needed for each testing condition so that the “wheel rotational differential” proof-of-concept is clearly demonstrated. This analysis allowed the researchers to decide, during ongoing testing as well, whether the estimated sample size enabled reliable and accurate statistical judgments, and if so, how the statistical test is able to detect the effects of a certain sample size for a particular test condition (e.g., road incline vs. flat, wet vs. snow, etc.) In this respect, a total of 30 vehicle passes were considered sufficient to verify hypotheses (i.e., null vs. alternative). These 30 vehicle passes were also compared against the results of 10 passes only. This way, statistical inferences could be drawn about test results under the four road surface conditions regarding differences or correlations between groups of data (e.g., dry vs. wet, etc.) Figure 35 presents preliminary statistical data for all four road surface conditions.

	Dry (S) - 10Runs	Dry (S) - 30Runs	Dry (F) - 15 Runs	LightWet - 10 Runs	LightWet - 30 Runs	VeryWet - 10 Runs	VeryWet - 30 Runs	WetSnow - 10 Runs	WetSnow - 30 Runs
	1.7149861705	1.7149861705	1.7153248056	1.7153971640	1.7148412997	1.7157564344	1.7150760719	1.7164029138	1.7148574287
	1.7152050473	1.7152050473	1.7151985967	1.7150213514	1.7152550892	1.7152376163	1.7153623917	1.7148569287	1.7149818818
	1.7149431165	1.7149431165	1.7151977967	1.7153826788	1.7151454363	1.7152734129	1.7151294295	1.7160571142	1.7155193992
	1.7153303076	1.7153303076	1.7152176640	1.7149304250	1.7144472362	1.7153971640	1.7151111669	1.7149298597	1.7152847153
	1.7148786316	1.7148786316	1.7150571393	1.7148059776	1.7144466700	1.7153826788	1.7157564344	1.7153257186	1.7148770697
	1.7149520928	1.7150094997	1.7151111669	1.7150375940	1.7152376163	1.7150213514	1.7152376163	1.7156112853	1.7164890282
	1.7147705845	1.7150429076	1.7152550892	1.7151477058	1.7152734129	1.7148968294	1.7152734129	1.7153431188	1.7164029138
	1.7156813627	1.7149861705	1.7157564344	1.7148765509	1.7153971640	1.7151842999	1.7153971640	1.7152351097	1.7148569287
	1.7157762414	1.7150605449	1.7152184832	1.7146977677	1.7150213514	1.7152168463	1.7153826788	1.7154654655	1.7160571142
	1.7150409062	1.7150402414	1.7152184832	1.7148604476	1.7153826788	1.7150936283	1.7150213514	1.7150025088	1.7149298597
		1.7157443590	1.7151111669		1.7149304250		1.7148968294		1.7153257186
		1.7154716981	1.7152359438		1.7148059776		1.7151842999		1.7156112853
		1.7153119093	1.7153440482		1.7150375940		1.7152168463		1.7153431188
		1.7148786316	1.7152010050		1.7151477058		1.7150936283		1.7152351097
		1.7153128153	1.7153074028		1.7148765509		1.7152742828		1.7154654655
		1.7153817130			1.7146977677		1.7152567976		1.7150025088
		1.7149861705			1.7148604476		1.7151111669		1.7156112853
		1.7149520928			1.7149122807		1.7153807489		1.7154278576
		1.7147705845			1.7150915016		1.7150025088		1.7158052809
		1.7156813627			1.7148217636		1.7152201258		1.7156101228
		1.7157762414			1.7150382541		1.7150409062		1.7157182251
		1.7150409062			1.7147697327		1.7148604476		1.7152351097
		1.7155561122			1.7146087175		1.7151636774		1.7152699486
		1.7151819322			1.7151827201		1.7152176640		1.7154685736
		1.7152050473			1.7142140258		1.7156147850		1.7154338817
		1.7148064354			1.7147339357		1.7153266332		1.7155226503
		1.7158531971			1.7143393393		1.7151118934		1.7152168463
		1.7152018106			1.7149685535		1.7152917505		1.7152690864
		1.7152018106			1.7150753769		1.7152243154		1.7155767541
		1.7155421535			1.7148050646		1.7151732648		1.7146966854
Samples =	10	30	15	10	30	10	30	10	30
Mean =	1.715156446	1.715211321	1.715250348	1.715015766	1.714912190	1.715246026	1.715213676	1.715423002	1.715403395
StdDev =	0.000341233	0.000300457	0.000160574	0.000234266	0.000298152	0.000236445	0.000193225	0.000493420	0.000421368
Variance.P =	0.0000001048	0.0000000873	0.0000000241	0.0000000494	0.0000000859	0.0000000503	0.0000000360	0.000000219	0.0000002191
Variance =	0.0000001164	0.0000000903	0.0000000258	0.0000000549	0.0000000889	0.0000000559	0.0000000348	0.000000243	0.0000002307

Source: VTTI

Figure 35. Screen capture. Preliminary statistical data pertaining to Smart Road testing using RWD vehicle.

To verify these assumptions, statistical tests such as Student's *t*-test and an analysis of variance (ANOVA) single-factor test were employed. These tests determine if two or more sets of data are significantly different from each other whether their means are equal or not.

Source: VTTI

Figure 36 and Figure 37 present statistical results of two-sample comparisons assuming unequal variances of the data. In this case, the null hypothesis states that all means are equal, whereas the alternative hypothesis states otherwise. The pre-specified level of significance for which the null hypothesis will be rejected is set at $\alpha = 0.05$, meaning that there is a 95% certainty that the null hypothesis is correct. In the *t*-test, paired sets of data were compared for different surface conditions and similar numbers of runs. The analysis showed that there were statistical differences between some of the surface conditions, but not all conditions. This indicates that the *t*-test is more powerful than the ANOVA single factor, which would only show differences among multiple data sets.

The paired *t*-tests in Figure 37 show that similar test results (i.e., no statistical differences exist) were recorded only for dry versus very wet surface conditions ($p > \alpha = 0.05$), all other comparisons rendering statistical differences. This is in accordance with the previous statement, which indicates adequate traction on clean roads when compared to the lightly wet dirty roads that are more slippery as a result of the "cleaning" effect of the front tires described above.

t-Test: Two-Sample Assuming Equal Variances			t-Test: Two-Sample Assuming Equal Variances		
	Dry (S) - 30Runs	*LightWet - 30 Runs*		*Dry (S) - 30Runs*	*Snow - 30 Runs*
Mean	1.715211321	1.71491219	Mean	1.715211321	1.715402546
Variance	9.02746E-08	8.88944E-08	Variance	9.02746E-08	1.68441E-07
Observations	30	30	Observations	30	30
Pooled Variance	8.95845E-08		Pooled Variance	1.29358E-07	
Hypothesized Mean	0		Hypothesized Mean Di	0	
df	58		df	58	
t Stat	3.870710019		t Stat	-2.059184811	
P(T<=t) one-tail	0.000138875		P(T<=t) one-tail	0.021987917	
t Critical one-tail	1.671552762		t Critical one-tail	1.671552762	
P(T<=t) two-tail	0.000277751	**P < α = 0.05 Reject**	P(T<=t) two-tail	0.043975835	**P < α = 0.05 Reject**
t Critical two-tail	2.001717484		t Critical two-tail	2.001717484	

t-Test: Two-Sample Assuming Equal Variances			t-Test: Two-Sample Assuming Unequal Variances		
	Dry (S) - 30Runs	*VeryWet - 30 Runs*		*LightWet - 30 Runs*	*VeryWet - 30 Runs*
Mean	1.715211321	1.715213676	Mean	1.71491219	1.71521474
Variance	9.02746E-08	3.48225E-08	Variance	8.88944E-08	3.73361E-08
Observations	30	30	Observations	30	28
Pooled Variance	6.25486E-08				
Hypothesized Mean	0		Hypothesized Mean Di	0	
df	58		df	50	
t Stat	-0.036479082		t Stat	-4.615680662	
P(T<=t) one-tail	0.485512811	**> α = 0.05 Accept**	P(T<=t) one-tail	1.38062E-05	
t Critical one-tail	1.671552762		t Critical one-tail	1.675905025	
P(T<=t) two-tail	0.971025622		P(T<=t) two-tail	0.0000276124	**P < α = 0.05 Reject**
t Critical two-tail	2.001717484		t Critical two-tail	2.008559112	

t-Test: Two-Sample Assuming Equal Variances			t-Test: Two-Sample Assuming Equal Variances		
	LightWet - 30 Runs	*Snow - 30 Runs*		*VeryWet - 30 Runs*	*Snow - 30 Runs*
Mean	1.71491219	1.715403395	Mean	1.715213676	1.715403395
Variance	8.88944E-08	1.77551E-07	Variance	3.48225E-08	1.77551E-07
Observations	30	30	Observations	30	30
Pooled Variance	1.33223E-07		Pooled Variance	1.06187E-07	
Hypothesized Mean	0		Hypothesized Mean Di	0	
df	58		df	58	
t Stat	-5.212186697		t Stat	-2.25486824	
P(T<=t) one-tail	0.00000130		P(T<=t) one-tail	0.013966007	
t Critical one-tail	1.671552762		t Critical one-tail	1.671552762	
P(T<=t) two-tail	0.00000259	**P < α = 0.05 Reject**	P(T<=t) two-tail	0.027932014	**P < α = 0.05 Reject**
t Critical two-tail	2.001717484		t Critical two-tail	2.001717484	

Source: VTTI

Figure 36. Screen capture. T-test analysis of Smart Road data (RWD).

Anova: Single Factor; **H0: All means are equal**						
SUMMARY						
Groups	*Count*	*Sum*	*Average*	*Variance*		
Dry (F) - 15 Runs	15	25.72875523	1.715250348	2.57842E-08		
LightWet - 30 Runs	30	51.44736569	1.71491219	8.88944E-08		
VeryWet - 30 Runs	28	48.02601271	1.71521474	3.73361E-08		
ANOVA						
Source of Variation	*SS*	*df*	*MS*	*F*	*P-value*	*F crit*
Between Groups	1.7655E-06	2	8.82749E-07	15.65557571	0.0000024012	3.127675601
Within Groups	3.94699E-06	70	5.63856E-08		**< α = 0.05 Reject**	
					F > Fcrit	
Total	5.71249E-06	72				
Anova: Single Factor						
SUMMARY						
Groups	*Count*	*Sum*	*Average*	*Variance*		
LightWet - 30 Runs	30	51.44736569	1.71491219	8.88944E-08		
VeryWet - 30 Runs	28	48.02601271	1.71521474	3.73361E-08		
WetSnow - 20 Runs	20	34.30869409	1.71543470	2.30652E-07		
ANOVA						
Source of Variation	*SS*	*df*	*MS*	*F*	*P-value*	*F crit*
Between Groups	3.43332E-06	2	1.71666E-06	16.15752326	0.0000014623	3.118642128
Within Groups	7.9684E-06	75	1.06245E-07		**< α = 0.05 Reject**	
					F > Fcrit	
Total	1.14017E-05	77				
Anova: Single Factor						
SUMMARY						
Groups	*Count*	*Sum*	*Average*	*Variance*		
Dry (S) - 30Runs	30	51.45633962	1.715211321	9.02746E-08		
VeryWet - 30 Runs	28	48.02601271	1.71521474	3.73361E-08		
WetSnow - 20 Runs	20	34.30869409	1.715434705	2.30652E-07		
ANOVA						
Source of Variation	*SS*	*df*	*MS*	*F*	*P-value*	*F crit*
Between Groups	7.31352E-07	2	3.65676E-07	3.424603589	0.037735881	3.118642128
Within Groups	8.00843E-06	75	1.06779E-07		**< α = 0.05 Reject**	
					F > Fcrit	
Total	8.73978E-06	77				

Source: VTTI

Figure 37. Screen capture. ANOVA single-factor analysis of Smart Road data (RWD).

A power analysis using the *t*-test that determines the statistical difference between data collected from 10 trips versus data collected from 30 trips for the same surface condition is presented in Figure 38. It can be seen from the table that the null hypothesis (i.e., H_0: all means are equal) was true in all the cases, as the *p*-values were significantly larger than the selected threshold, α = 0.05. This analysis also controls for the probability of a type I error occurring (i.e., accepting a false null hypothesis), thus rejecting a true alternative hypothesis under identical testing conditions.

t-Test: Two-Sample Assuming Unequal Variances			t-Test: Two-Sample Assuming Unequal Variances		
	Dry (S) - 10Runs	*Dry (S) - 30Runs*		*VeryWet - 10 Runs*	*VeryWet - 30 Runs*
Mean	1.715156446	1.715211321	Mean	1.715246026	1.71521474
Variance	1.1644E-07	9.02746E-08	Variance	5.59064E-08	3.73361E-08
Observations	10	30	Observations	10	28
Hypothesized Me	0		Hypothesized Mean	0	
df	14		df	14	
t Stat	-0.4533215		t Stat	0.375990257	
P(T<=t) one-tail	0.328632011		P(T<=t) one-tail	0.356280158	
t Critical one-tail	1.761310136		t Critical one-tail	1.761310136	
P(T<=t) two-tail	**0.657264021**	**> α = 0.05 Accept**	P(T<=t) two-tail	**0.712560317**	**> α = 0.05 Accept**
t Critical two-tail	2.144786688		t Critical two-tail	2.144786688	
t-Test: Two-Sample Assuming Unequal Variances			t-Test: Two-Sample Assuming Unequal Variances		
	LightWet - 10 Runs	*LightWet - 30 Runs*		*WetSnow - 10 Runs*	*WetSnow - 30 Runs*
Mean	1.715015766	1.71491219	Mean	1.715423002	1.715434705
Variance	5.48808E-08	8.88944E-08	Variance	2.43463E-07	2.30652E-07
Observations	10	30	Observations	10	20
Hypothesized Me	0		Hypothesized Mean	0	
df	20		df	18	
t Stat	1.126683575		t Stat	-0.061780632	
P(T<=t) one-tail	0.13660685		P(T<=t) one-tail	0.475709184	
t Critical one-tail	1.724718243		t Critical one-tail	1.734063607	
P(T<=t) two-tail	**0.2732137**	**> α = 0.05 Accept**	P(T<=t) two-tail	**0.951418367**	**> α = 0.05 Accept**
t Critical two-tail	2.085963447		t Critical two-tail	2.10092204	

Source: VTTI

Figure 38. Screen capture. Statistical power for calculating differences in sample size for Smart Road data (RWD).

Figure 39 presents statistical inferences for the data collected on U.S. Route 460-E for three surface conditions while driving the RWD vehicle. The *t*-test analysis indicated that there was a statistical difference between the dry and very wet data results (probability value – $p < \alpha$). No significant differences were observed between dry and slushy conditions ($p > \alpha = 0.05$). Marginal differences existed between very wet and slushy conditions as indicated by the *t*-test (one-tail) and ANOVA single factor (*F*-stat > *F*-critical and $p < \alpha$). The borderline difference between the two conditions was due to the fact that in both cases the surface was free of contaminants (i.e., as opposite to a slightly wet surface) and the water accumulation did not meet hydroplaning conditions. In other words, the water layer on the road surface was virtually similar for both the wet and slushy conditions. Also, the slush layer was not uniform nor very consistent as the temperature was on the rise. However, the ANOVA statistic indicated that at least two conditions were equivalent as showed by the *p*-value ($\alpha < 0.068$).

	460E - Dry	460E - VWet	460E - Slush
	1.71857051	1.71824703	1.71825208
	1.71848894	1.71827173	1.71795187
	1.71863246	1.71828410	1.71822441
	1.71779093	1.71841255	1.71821072
	1.71872840	1.71848075	1.71831722
	1.71860247	1.71829904	1.71820878
	1.71839460	1.71830791	1.71841373
	1.71862111	1.71828367	1.71832655
	1.71838697	1.71784914	1.71828418
	1.71866475	1.71825440	1.71845214
Samples =	10	10	6
Mean =	1.718488115	1.718269031	1.718264168
StdDev =	0.000269233	0.000165089	0.000137435
Variance.P =	0.0000000652	0.0000000245	0.0000000170
Variance =	0.0000000725	0.0000000273	0.0000000189

t-Test: Two-Sample Assuming Unequal Variances

	460E - Dry	460E - VWet
Mean	1.718488115	1.718269031
Variance	7.24863E-08	2.72545E-08
Observations	10	10
Hypothesized Mean	0	
df	15	
t Stat	2.193678989	
P(T<=t) one-tail	0.022214042	
t Critical one-tail	1.753050356	
P(T<=t) two-tail	0.044428084	P < α = 0.05 Reject
t Critical two-tail	2.131449546	

t-Test: Two-Sample Assuming Equal Variances

	460E - Dry	460E - Slush
Mean	1.71847896	1.718265512
Variance	8.06042E-08	2.12291E-08
Observations	9	9
Pooled Variance	5.09167E-08	
Hypothesized Me	0	
df	16	
t Stat	2.006634717	
P(T<=t) one-tail	0.030997145	P < α = 0.05 Reject
t Critical one-tail	1.745883676	
P(T<=t) two-tail	0.06199429	
t Critical two-tail	2.119905299	

t-Test: Two-Sample Assuming Equal Variances

	460E - VWet	460E - Slush
Mean	1.718269031	1.718550856
Variance	2.72545E-08	1.24086E-07
Observations	10	6
Pooled Variance	6.18372E-08	
Hypothesized Mean	0	
df	14	
t Stat	-2.19467265	
P(T<=t) one-tail	0.02277638	P < α = 0.05 Reject
t Critical one-tail	1.761310136	
P(T<=t) two-tail	0.045552759	
t Critical two-tail	2.144786688	

Anova: Single Factor

SUMMARY

Groups	*Count*	*Sum*	*Average*	*Variance*
460E - Dry	9	15.46631064	1.71847896	8.06042E-08
460E - VWet	9	15.46444328	1.718271475	3.05941E-08
460E - Slush	9	15.46438961	1.718265512	2.12291E-08

ANOVA

Source of Variation	*SS*	*df*	*MS*	*F*	*P-value*	*F crit*
Between Groups	2.65936E-07	2	1.32968E-07	3.012249404	0.06804962	3.402826105
Within Groups	1.05942E-06	24	4.41425E-08		P > α = 0.05 Accept	
Total	1.32536E-06	26				

Source: VTTI

Figure 39. Screen capture. Statistical analysis *t*-test and ANOVA of 460-E data (RWD).

In this particular statistical experiment, it must be ensured that the power analysis would be reasonably high to detect significant departures from the null hypothesis (H_0). Because of the nature of the testing, the accept-support (AS) type of null hypothesis can be considered as either all the relative displacements or ratios pertaining to a specific test condition are less than 1 or they differ among each other. The alternative hypothesis (H_1) only assumes the opposite is true or that the differences in rotation between driven (or free-rolling) and driving (or non-driven) wheels will equal zero and it should be rejected (i.e., accepted only if H_0 is rejected). It also indicates the probability of accepting a false null hypothesis, which is a type II error or (β) (i.e., power is equal to 1 - β). In doing this, the magnitude of the difference in rotation or distance traveled between driven and nondriven wheels had to be analyzed.

Chapter 4. Lessons Learned

Several lessons were learned during the course of this study that should provide useful insights for future road-surface testing using this concept and for various transportation agencies that may seek to implement the method proposed herein. They include the following:

- The polarized retroreflective laser sensor used to measure the distance the vehicle traveled presented irregular latencies in object detection, introducing detrimental measurement errors due to unsynchronized triggers in the data collection. Several attempts to remedy the problem were unsuccessful; therefore the laser system has been considered unsuitable for further distance measurements.

- The differential GPS service employed to determine traveled distance showed some variability in the dynamic test results but the static measurements for geofencing (i.e., delineating the start and end positions of the traveled distance) provided adequate accuracy (± 2-3 inch variation). For this reason, multiple readings were taken and averaged to obtain accurate coordinates for the start and end locations.

- Swapping tires front to rear and side to side to account for tire diameter variation, for both FWD and RWD vehicles, did not affect any of the test distance measurements. For this purpose, a 50-m distance was manually measured and then traveled several times while wheel revolutions were recorded. The tire pressure was the same as for the actual testing sessions.

- Also, decreasing the tire pressure by a few psi (e.g., 2 to 3 psi) on one or two tires at the same time and traveling the same 50-m distance multiple times did not affect the wheel revolutions. Similar behavior has been reported in the literature.

Chapter 5. Summary and Conclusions

This report describes a new methodology aimed at evaluating real-time road surface conditions using data supplied by the wheel-speed sensors of a vehicle. In this respect, wheel pulse data acquired through the vehicle CAN, along with other parameters, could be used as a new tool to effectively detect slippery, and thus hazardous, road conditions. The information can be shared among vehicles traveling in certain locations by using CV technology so that warnings or alerts will be issued to drivers to caution them about the imminent dangers. This technology could also help to more effectively mitigate speed-related crashes or crash severity and to further reduce the costs associated with these crashes in the United States and worldwide, particularly when combined with other weather-responsive, traffic-management strategies. Although it is difficult at this stage to make definitive assertions with respect to the evaluation of the road friction characteristics using vehicle onboard sensors, some progress was made toward this objective through this research study.

General findings based on the overall results from the study include the following:

- Based on the wheel rotational data provided by the two types of vehicles, the FWD and RWD, it can be inferred that the driven wheels rotate more than the free-rolling wheels over the same distance on different road surface conditions. Calculated ratios that were less than 1 for nondriven-to-driven traveled distances confirmed this finding. This means that the micro-slippage that occurs at the driven wheels is more pronounced than that at the free-rolling wheels. Furthermore, these ratios can be used as “traction” indices to relatively differentiate among road surface conditions in a timely manner.

- For the RWD vehicle, the calculated nondriven-to-driven ratios for wet and icy road surfaces were less than the ratio calculated for a dry road surface. This trend indicates that for these particular slippery road conditions the driven wheels are spinning much more than the free-rolling wheels. For the road surface covered by snow, the ratios were slightly larger than those calculated for the dry surface. This specific difference indicates that there was also a proportional increase in slippage (i.e., increase in wheel pulses) at the free-rolling wheels.

- Similar nondriven-to-driven ratio trends for the RWD vehicle were observed under wet/slushy road conditions for the less-inclined (below 2% grade) and lengthier road section on U.S. Route 460-E. In this case, although the driven axle exhibited more rotation on the wet/slushy road surface than on the dry surface, a proportional increase in wheel pulses also occurred at the free-rolling axle, thus leading to a slight jump in the overall ratio.

- For the FWD vehicle, the calculated ratios were also less than 1, showing that more rotation, hence more wheel travel, occurred at the driven wheels compared with the nondriven wheels. For this case, however, the ratios corresponding to the wet surface conditions were slightly higher than those for dry surface, indicating, again, that both driven and nondriven axle pulses increased proportionally. Similar to the RWD vehicle testing, the pulse ratio for the icy surface was the lowest, showing that more rotation occurred at the driven (i.e., front) axle compared with the free-rolling axle.

References

Alimasi, N., S. Takahashi, and H. Enomoto. 2012. *Development of a Mobile Optical System to Detect Road-Freezing Conditions.* Bulletin of Glaciological Research, 30, 41-51.

Andersson, M., F. Bruzelius, J. Casselgren, M. Gäfvert, M. Hjort, J. Hultén, F. Håbring,M. Klomp, G. Olsson, M. Sjödahl, J. Svendenius, S. Woxneryd, and B. Wälivaara. 2007. *Road Friction Estimation.* IVSS Project Report 17750.

Askelson, M. A. 2008. *The Pavement Precipitation Accumulation Estimation System.* Transportation Research Board, Washington, D. C., June 16-19, 2008, Indianapolis, Indiana: Transportation Research Circular No. E-C126, Surface Transportation Weather and Snow Removal and Ice Control Technology, Seventh International Symposium on Snow Removal and Ice Control Technology.

Blau, P. J. 2009. *Friction Science and Technology, From CONCEPTS to APPLICATIONS, .* Boca Raton, FL: Society of Tribologists and Lubrication Engineers, CRC Press, Taylor & Francis group.

Blincoe, L. J., A. Seay, E. Zaloshnja, T. Miller, E. Romano, S. Luchter, R. Spicer. 2002. *The Economic Impact of Motor Vehicle Crashes.* 2000, NHTSA Technical Report, Report No. DOT HS 809 446.

Blundell, M. and D. Harty. 2004. *The Multibody Systems Approach to Vehicle Dynamics.* Oxford, UK: Butterworth-Heinemann, Elsevier.

Boon, C. B. and C. Cluett. 2002. *Road Weather Information Systems: Enabling Proactive Maintenance Practices in Washington State.* Washington State Department of Transportation, Report WA-RD 529.1.

Bullas, J. C. 2004. *Tires, Road Surfaces, and Reducing Accidents: A Review.* UK: Foundation for Road Safety Research, The County Surveyors' Society.

Carlson, C. R., J. C. Gerdes, and J. D. Powell. 2003. *Error Sources with Land Vehicle Dead Reckoning with Differential Wheel Speeds.* Stanford University, Stanford, California.

Clark, S. K. 1971. *Mechanics of Pneumatic Tires, National Bureau of Standards Monograph 122.* Ann Arbor, MI.: National Highway Traffic Safety Administration.

Dawkins, J., R. Bishop, B. Powell, and D. Bevly. 2011. "Investigation of Pavement Maintenance Applications of IntellidriveSM(Final Report): Implementation and Deployment Factors for Vehicle Probe-Based Pavement Maintenance (PBPM)." Auburn University.

Erdogan, G., L. Alexander, P. Agrawal, and R. Rajamani. 2007. *Automated Winter Road Maintenance Using Road Surface Condition Measurements.* Minnesota Department of Transportation Final Report MN/RC 2007-37.

Erkkilä, K., P. Laine, N.-O. Nylund, P. Silvonen, T. Murtonen, M. Lappi, M. Juhala, M.Laamanen, J. Kankare, T. Naskali, K. Noponen, H. Liimatainen, and R. Wahlsten. 2012. *Energy Efficient and Intelligent Heavy Vehicle.* VTT-R-08344-12, HDENIQ Final Report 2012.

Gabriel, P., A. G. Thomas, and J. J. C. Busfield. 2010. "Influence of Interface Geometry on Rubber Friction, Wear, 268, 747-750."

Giessler, M., F. Gauterin, K. Wiese, and B. Wies. 2010. *Influence of Friction Heat on Tire Traction on Ice and Snow.* Tire Science and Technology, TSTCA, 38 (1), 4-23.

Gillespie, T. D. 1992. *Fundamentals of Vehicle Dynamics.* (SAE), Warrendale, PA: Society of Automotive Engineers .

Gustaffson, F. 1997. *Slip-Based Tire-Road Friction Estimation.* Automatica, 33(6), 1087–1099.

Haavasoja, T. and Y. Pilli-Sihvola. 2010. *Friction as a Measure of Slippery Road Surfaces.* Finland: Teconer Oy, Helsinki, Finnish Road Administration.

Hall, J. W., K. L. Smith, L. Titus-Glover, J. C. Wambold, T. J. Yager, and Z. Rado. 2009. *Guide for Pavement Friction.* NCHRP Web-Only Document 108, Final Report for NCHRP Project 01-43.

Hay, C. 2005. *Turn, Turn, Turn - Wheel-Speed Dead Reckoning for Vehicle Navigation.* GPS World, 37-42.

Heising, B. and M. Ersoy. 2011. *Chassis Handbook: Fundamentals, Driving Dynamics, Components, Mechatronics, Perspectives, .* Vieweg Teubner, Springer Fachmedien Wiesbaden GmbH 2011.

Henry, J. J. 2000. *Evaluation of Pavement Friction Characteristics.* Washington, D.C.: NCHRP Synthesis 291 National Cooperative Highway Research Program (NCHRP).

2010. *IIHS Status Report.* Insurance Institute for Highway Safety, Vol. 45, No. 10.

IRIBA. 2012. *Mobile Friction Solution (µTEC) and Mobile Friction Measurement System (MµMS), TECONER OY.* Technical Consulting and Research.

Knight, P. G., J. Aguero-Valverde, and P. P. Jovanis. 2008. *Advanced Road Safety and Weather Warning System.* Washington, D. C.: Transportation Research Circular No. E-C126, Surface Transportation Weather and Snow Removal and Ice Control Technology, Seventh International Symposium on Snow Removal and Ice Control Technology, Transportation Research Board.

Kumagai, N., S. Uchida, I. Hasegawa, and K.Watanabe. 2000. *Wheel Slip Rate Control Using Synchronized Speed Pulse Computing.* Computers in Railways VII, WIT Press, 623-632.

Malmivuo, M. 2013. *Comparison Study of Mobile Optical Friction and Temperature Meters.* Finnish Transport Agency, Innomikko Ltd, Report 2013-52.

Malmivuo, M. n.d. *Friction Meter Comparison Study 2011, .* Helsinki, 23-25 May, 2012: SIRWEC Conference.

Milliken, W. F. and D. L. Milliken. 1995. "Race Car Vehicle Dynamics." *SAE International, Warrendale, PA.*

Moore, D. F. 1975. "The Friction of Pneumatic Tyres." *Elsevier Scientific Publishing Company, The Netherlands.*

Muller, S., M. Uchanski, and K. Hedrick. 2003. *Estimation of the Maximum Tire-Road Friction Coefficient.* J. of Dynamic Systems, Measurement, and Control, 125, 607-617.

Murphy, R., R. Swick, and G. Guevara. 2012. *Best Practices for Road Weather Management.* Version 3.0, FHWA, Report No. FHWA-HOP-12-046.

Nakatsuji, T. and A. Kawamura. 2003. *Relationship between Winter Road Surface Conditions and Vehicular Motions Measured by GPS-Equipped Probe Vehicles.* Washington, D.C. : TRB, 82nd Annual Meeting.

Noyce, D. A., H. U. Bahia, J. Yambo, J. Chapman, and A. Bill. 2007. *Incorporating Road Safety into Pavement Management: Maximizing Surface Friction for Road Safety Improvements.* Wisconsin Department of Transportation, Report No. MRUTC 04-04.

Pacejka, H. B. and I. Besselink. 2012. *Tyre and Vehicle Dynamics, Butterworth-Heinemann.* Oxford, UK: Butterworth-Heinemann, 3rd Ed., Elsevier.

Persson, B. N. J. 1998. *On the Theory of Rubber Friction.* Surface Science, 401, 445-454.

Petersen, I. 2003. *Wheel Slip Control in ABS Brakes using Gain Scheduled Optimal Control with Constraints.* Trondheim, Norway: Doctoral Dissertation, Norwegian University of Science and Technology.

Pilli-Sihvola, E., R. Hautala and P. Leviäkangas. 2014. *New Ways of Providing and Taking Advantage of Road Weather Information.* Washington D.C.: Paper submitted to TRB 93rd Annual Meeting.

Pisano, P. 2011. *Road Weather and the Connected Vehicle.* Publication No. FHWA-JPO-11-138.

Pyykonen, P., J. Laitinen, P. Eloranta, T. Korhonen. 2013. *Road Friction Monitoring In Intelligent Traffic System, Workshop, Best Practices on Deployment of Monitoring Technologies and Services.* Espoo, Finland. : VTT - Technical Research Centre.

Rajamani, R. 2012. *Vehicle Dynamics and Control.* New York, USA: Springer, 2nd Ed.

Rall, J. 2012. *Weather or Not? State Liability and Road Weather Information Systems.* April 30–May 3, 2012, Coralville, Iowa: Transportation Research Circular No. E-C162, Winter Maintenance

and Surface Transportation Weather, International Conference on Winter Maintenance and Surface Transportation Weather.

Savaresi, S. M. and M. Tanelli. 2010. *Active Braking Control Systems Design for Vehicles.* London, UK: Springer-Verlag.

Singh, K. B., M. Arat, and S. Taheri. 2013. *An Intelligent Tire Based Tire-Road Friction Estimation Technique and Adaptive Wheel Slip Controller for Antilock Brake System.* J. of Dynamic Systems, Measurement, and Control, 135, 1-26.

Smith, R. H. 2008. *Analyzing Friction in the Design of Rubber Products and Their Paired Surfaces.* Boca Raton, FL: CRC Press, Taylor & Francis Group.

Smithson, L. 2012. *ptimized and Sustainable Winter Operations in Canada and the United States, Paper presented at the Innovations and Opportunities in Maintenance Methods and Practices.* New Brunswick: Session of the 2012 Conference of the Transportation Association of Canada Fredericton.

2006. *The Pneumatic Tire.* National Highway Traffic Safety Administration, U.S. Department of Transportation, NHTSA Report No. DOT HS 810561.

2006. *The Pneumatic Tire, U.S. Department.* National Highway Traffic Safety Administration, NHTSA Report No. DOT HS 810561.

Wang, H., Al-Qadi, I. and Stanciulescu, I. 2010. *Effect of Friction on Rolling Tire Pavement Interaction U.S. DOT Region V Regional University Transportation Center Final Report.* Nextrans Project No. 049IY02, Nextrans Center.

Wang, L., M. Hui, and H. Zongqi. 2014. *Fast Fourier Transformation Processing Method for Wheel Speed Signal.* American Journal of Engineering Research, 3 (1), 35-42.

Wayson, R. L. 1998. *Relationship Between Pavement Surface Texture and Highway Traffic Noise.* Washington, D.C: NCHRP, Synthesis of Highway Practice 268, TRB, National Academy Press, .

Wong, J. Y. 2001. *Theory of Ground Vehicles, 3rd Ed.* NY: Wiley & Sons.

APPENDIX A. List of Acronyms

4WD	Four-wheel Drive
ABS	Antilock Braking System
AWD	All-wheel Drive
CAN	Controller Area Network
CV	Connected vehicle
DAS	Data acquisition system
DGPS	Differential Global Positioning System
DSRC	Dedicated Short Range Communications
ESC	Electronic Stability Control
FFT	Fast Fourier Transform
FHWA	Federal Highway Administration
FWD	Front-wheel Drive
GNSS	Global Navigation Satellite System
GPS	Global Positioning System
IMU	Inertial Measurement Unit
OBE	Onboard equipment
RDD	Relative Driver Displacement
RND	Relative Nondriver Displacement
RRD	Relative Rotational Displacement
RSE	Roadside equipment
RWD	Rear-wheel Drive
SSD	Solid-state drive
SUV	Sport-Utility Vehicle
TCS	Traction Control System
VTTI	Virginia Tech Transportation Institute

APPENDIX B. Tire Parameters

Table B-1. Tire parameters for Smart Road testing (Chevy Tahoe).

Tire Parameter	Pavement condition	Left Front	Left Front	Right Front	Right Front	Left Rear	Left Rear	Right Rear	Right Rear
		Side	Tread	Side	Tread	Side	Tread	Side	Tread
Temperature (°C)	Dry Pavement Surface (Sep 2013)	21.8	20.1	21.1	18.4	21.5	21.1	20.7	19.9
Pressure (psi)*	Dry Pavement Surface (Sep 2013)	37	37	37	37	37	37	37	37
Temperature	Slightly Wet Pavement Surface (Oct 2013)	22.3	18.7	21.1	16.7	16.2	15.8	17.1	15.2
Temperature	Very Wet Pavement Surface (Oct 2013)	21.6	20.1	23.4	21.6	21.8	21.9	20.8	19.7
Temperature	Icy Pavement Surface (Feb 2014)	9.3	2.4	10.1	2.6	2.3	0.8	2.6	0.9
Temperature	Snowy Pavement Surface (Mar 2014)	8.4	6.2	7.1	6.4	7.4	6.4	6.8	5.7

* Tire pressure was kept at 37 psi for all testing conditions.

Table B-2. Tire parameters for Smart Road testing (Chevy Impala).

Tire Parameter	Pavement Condition	Left Front	Left Front	Right Front	Right Front	Left Rear	Left Rear	Right Rear	Right Rear
		Side	Tread	Side	Tread	Side	Tread	Side	Tread
Temperature (°C)	Dry Pavement Surface (Feb 2014)	13.6	12.4	13.8	12.4	8.7	7.8	8.6	7.7
Pressure (psi)*	Dry Pavement Surface (Feb 2014)	37	37	37	37	37	37	37	37
Temperature	Slightly Wet Pavement Surface (Mar 2014)	12.6	11.5	13.4	10.3	10.2	9.6	10.4	9.2
Temperature	Very Wet Pavement Surface (Mar 2014)	14.6	13.8	14.8	13.5	12.7	10.9	13.2	12.6
Temperature	Icy Pavement Surface (Feb 2014)	7.2	1.8	6.8	1.4	6.5	1.2	6.4	1.1
Temperature	Snowy Pavement Surface (Mar 2014)	6.9	5.8	6.3	5.9	7.1	6.6	6.4	5.9

APPENDIX C. Weather Parameters

Table B-3. Site weather parameters for the Smart Road testing (Chevy Tahoe).

Pavement Surface Condition	Air Temperature (°C)	Road Temperature (°C)	Wind (mph)	Dew Point	Humidity (%)
Dry	16.7	13.9	1.2	12.4	81.8
Slightly Wet	14.6	13.2	7.2	5.8	53.4
Very Wet	13.9	10.5	2.5	13.2	89.7
Ice	-7.8	-13.8	0.4	-16	37.4
Snow	-3.6	-4.2	1.7	1.3	97.2

Table B-4. Site weather parameters for Smart Road testing (Chevy Impala).

Pavement Surface Condition	Air Temperature (°C)	Road Temperature (°C)	Wind (mph)	Dew Point	Humidity (%)
Dry	2.6	3.7	0.9	-10.8	36.6
Slightly Wet	0.6	3.7	6.7	-14.9	38.6
Very Wet	7.3	9.5	6.4	1.4	71.3
Ice	-8.1	-14.4	0.3	-17	37.6
Snow*	-	-	-	-	-

* No testing was conducted in snow using the Chevy Impala

U.S. Department of Transportation
ITS Joint Program Office-HOIT
1200 New Jersey Avenue, SE
Washington, DC 20590

Toll-Free “Help Line” 866-367-7487
www.its.dot.gov

FHWA -JPO-16-359

U.S. Department of Transportation